Wide Bandgap Devices in AC Electric Drives: Opportunities and Challenges

[1]Ajay Morya†, *Member, IEEE*, [1]Matthew C. Gardner, *Student Member, IEEE,* [2]*Bahareh Anvari, Member, IEEE,* [2]*Liming Liu, Senior Member, IEEE* [3]Alejandro G. Yepes, *Member, IEEE,* [3]Jesus Doval-Gandoy, *Member, IEEE,* [1]Hamid A. Toliyat, *Fellow, IEEE*
[1]Advanced Electric Machines & Power Electronics (EMPE) Lab
Department of Electrical and Computer Engineering
Texas A&M University
College Station, Texas 77843
†ajay.morya@tamu.edu
[2]ABB Inc.
Raleigh, USA
[3]Applied Power Electronics Technology (APET) Research Group
Department of Electronics Technology
University of Vigo

***Abstract*—Wide bandgap (WBG) device-based power electronics converters are more efficient and lightweight than Silicon-based converters. WBG devices are an enabling technology for many motor drive applications and new classes of compact and efficient motors. This paper reviews the potential applications and advances enabled by WBG devices in ac motor drives. Industrial motor drive products using WBG devices are reviewed and the benefits are highlighted. This paper also discusses the technical challenges, converter design considerations and design trade-offs in realizing the full potential of WBG devices in motor drives. There is a trade-off between high switching frequency and other issues such as high *dv/dt* and electromagnetic interference. The problems of high common mode currents and bearing and insulation damage, which are caused by high *dv/dt*, and the reliability of WBG devices are discussed.**

***Index Terms*—Electric vehicle (EV), electromagnetic compatibility (EMC), electromagnetic interference (EMI), gallium nitride (GaN), integrated motor drive (IMD), low-inductance motors, MW level high-speed motors, reliability, silicon carbide (SiC), slotless motor, wide bandgap (WBG) device.**

I. Introduction

Significant research efforts have been focused on the development of wide bandgap (WBG) semiconductor devices [1]-[3] and their applications in power electronics [4]. The Advanced Research Projects Agency–Energy (ARPA-E) of the United States (US) Department of Energy (DOE) is working to improve the energy efficiency and develop advanced power conversion technologies. To achieve these goals, ARPA-E created the CIRCUITS program to sponsor the development of next-generation efficient, lightweight, and reliable power converters based on WBG devices for use in industrial, automotive, ship propulsion, aerospace, and rail applications [5]. The Silicon Carbide application working group (SiC AWG) of the international technology roadmap for WBG power semiconductors is working with industry and academia to develop a long term vision for the adoption of SiC in various power conversion applications. This involves identifying the impact of WBG devices on performance across a range of applications and developing the device criteria that manufacturers must achieve to enable SiC devices to realize their benefits fully [6].

The primary advantages of WBG devices result from their low losses, high switching frequency and high-temperature operation capability [3], [4].

SiC and Gallium Nitride (GaN) are the two most prominent WBG materials for power devices. Lateral GaN devices are available for voltages up to 650 V. Vertical GaN devices, which are currently under development, will be able to operate at higher voltages [7]. SiC devices can operate at even higher voltages [8]. The design and manufacturing challenges for very high voltage modules are currently limiting SiC devices from achieving their maximum potential [9]. Wolfspeed has developed an evaluation module for a 10 kV SiC MOSFET and 24 kV SiC insulated gate bipolar transistors (IGBT) for 200 °C temperature operation; however, the performance of the IGBT degraded at temperatures above 125 °C during testing [9].

Characterizations of the switching loss, turn-on and turn-off times, and static characteristics, such as forward conduction and transfer characteristics, of WBG devices are widely available in literature [10]-[14]. Various design considerations, such as gate driver design, layout design, and thermal management, for voltage source converters using WBG devices are described in [11].

WBG devices have numerous applications in motor drives [15]. These WBG devices can provide significant benefits for many applications, especially low-inductance motors, high-speed motors, and electric drives operating in high-temperature environment, as shown in Fig. 1. WBG devices are enabling high power, low-inductance motors that require a high switching frequency and a high-bandwidth current

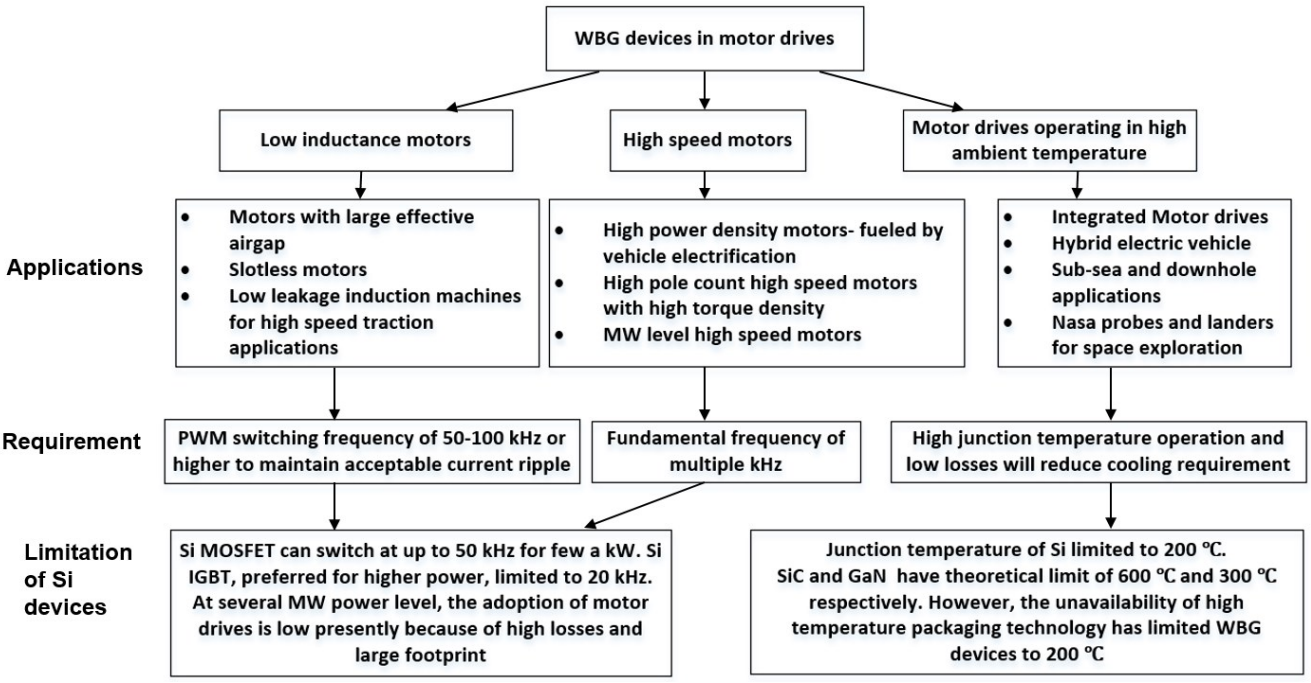

Fig. 1. Applications of WBG devices in ac motor drives.

regulation strategy to obtain an acceptable current ripple. The current ripple requirement is typically lower than 5% for many applications [16]. Along with the recent technological advances in motors, SiC devices are enabling the next generation of high-speed direct-drive medium-voltage drives for megawatt (MW) class motors in many critical energy applications. The dominant application areas are petroleum refining industries, natural gas infrastructure, and other industrial applications. Additionally, the demand for high-speed motors for drilling, milling, grinding, and machining applications, turbo compressors, and flywheels is increasing [17]. WBG-based converters have lower losses at the high switching frequencies required for these motors when compared to Silicon (Si)-based converters. This makes the system more efficient, light-weight, and compact, which is particularly important in portable applications. Another class of electric drive benefitting from WBG devices is motor drives operating in high-temperature environments. Hybrid electric vehicles (HEVs), sub-sea and down-hole pump applications, deep earth drilling, combat electric vehicles (EVs), spacecraft, and NASA probes and landers for space exploration are typical examples of drives in high-temperature environment [18]-[20].

The increase of the switching speed in power devices increases the power density of power electronic converters as it reduces the weight and volume of passive components [21], [22]. Significant research efforts are reported for designing high performance gate drivers [23]-[27], for analyzing the effects of the parasitic inductance and capacitance on the converter performance [28]-[31], for integrating the gate driver and the SiC MOSFET inside the module to minimize the gate-source parasitic inductance [32], and for designing the SiC MOSFET module and dc link bus bar to achieve a low stray inductance [33]. There are some papers that address the complete design of converters with WBG devices [11], [34]-[35]. The characteristics of GaN and challenges encountered in GaN-based converter design are reviewed in [36]. High *dv/dt* excites the capacitive coupling paths in the converter, cables and motor causing substantial common-mode (CM) current to flow, which can damage the motor bearings. The fast switching speed of WBG devices presents a challenge for the insulation design of voltage source inverter (VSI)-fed motors, particularly for the interturn insulation [37].

While some papers describe the performance improvements of motor drives using WBG devices in individual applications, the literature lacks a thorough review providing the different major ac motor drive applications that would benefit from WBG devices. This paper addresses this issue. The hurdles and technical challenges in realizing the full potential of WBG devices in motor drives are also discussed.

Section II reviews the electric drives enabled by WBG devices and their potential applications. Section III reviews the recent industrial motor drive products using WBG devices. Section IV discusses the problems caused by high *dv/dt* of WBG devices in motor drives, the trade-off between high switching frequency and EMI, and the packaging issues for high voltage and high temperature devices. Section V reviews and discusses the specific gate driver design, power circuit

TABLE I
PROPERTIES OF WIDE BANDGAP DEVICES

Property	Si	GaN	SiC
Bandgap (eV)	1.1	3.4	3.2
Electron mobility (cm^2/Vs)	1450	2000	900
Critical electric field (MV/cm)	0.3	3.5	3.0
Electron saturation velocity (10^7 cm/s)	1.0	2.5	2.2
Thermal conductivity (W/cm-K)	1.5	1.3	5.0
Maximum operating temperature (°C)	200	300	600
Specific heat capacity (J/KgK)	712	490	681

design, short circuit protection requirement, and reliability of WBG devices.

II. APPLICATIONS OF WBG DEVICES IN AC ELECTRIC DRIVES

Some important properties of Si, SiC and GaN are shown in Table I. The WBG materials have a higher critical electric field (≥ 200 V/μm) than Si, which has a critical electric field of 30 V/μm. This makes it possible to design thinner and more highly doped voltage-blocking layers, which can reduce on-resistance by two orders of magnitude compared to Si in majority carrier devices like MOSFETs [3]. The low intrinsic carrier concentration of WBG materials, which is less than $10^{-9}/cm^3$, results in low leakage currents, even at high temperatures, which enables robust high-temperature performance [3]. The figure of merit (FOM) is defined as the product of the on-state resistance and gate charge for a switch, so a lower FOM corresponds to better performance [38]. WBG devices have much lower FOMs than Si devices. For example, a GaN transistor has three to seven times better FOM than a Si MOSFET [38].

A. Low-Inductance Motors

Low-inductance motors generally require a pulse width modulation (PWM) frequency of 50-100 kHz or higher to keep the current ripple within acceptable limits [39]. Current ripple is unwanted because it wastes energy in the motor windings and may cause torque pulsations.

Slotless motors are another typical example of low-inductance motors. ThinGap designs high performance motors with ironless composite stators [40]. These motors have low inductances ranging from 10-100 μH [41] and require high PWM switching frequencies. Motors having ironless composite stators are very good in applications requiring torque linearity, velocity smoothness, positioning accuracy, extremely small cogging torque, and a high power-to-weight ratio [40]. These features make ironless motors extremely suitable for industrial applications like unmanned systems, aerospace, defense, precision manufacturing, EVs, and portable industrial applications [40].

Surface-mounted permanent magnet (SMPM) motors have a low inductance due to their long effective air gap [39]. High-speed PM brushless dc (BLDC) motors are compact, reliable, and efficient. These motors generally have a low inductance, and making them ironless further reduces the inductance [42]-[44], sometimes to less than 100 μH [42]. Reliability, direct-drive capability, high-efficiency, and high dynamic performance requirements are important for turbomachinery [45]. These requirements are also driving research in high-power slotless motors [45]. For low-inductance motors rated at a few kilowatts, Si MOSFETs can be used because they can provide the desired current ripple by switching at up to 50 kHz frequency [42]. At power levels higher than a few kilowatts, Si IGBTs are preferred over MOSFETs, but the switching frequency of a Si IGBT is limited to about 20 kHz [42] which fails to meet the current ripple limitations in low-inductance motors. Thus, due to their high switching frequency capability, WBG devices enable low-inductance motors rated for high power.

The maximum speed at which a given motor can provide sufficient power is directly related to the bus voltage and the back EMF constant. In general, reducing the leakage inductance of an induction machine increases its constant-power speed range relative to its base speed [16]. This is highly desirable for high-speed traction motors [16]. WBG devices are critical for driving such low-inductance motors, especially at high speeds.

B. High-Speed Motors

High-speed electric machines are gaining popularity in industry due to their high power density [17]. High-speed machines are mainly used in EVs, more-electric aircraft, flywheel energy storage systems, high-speed spindle applications, gas compressors, industrial air compressors, and air blowers [17].The worldwide push for electrification of transportation systems is also fueling the advance of high-speed machine technologies. The fundamental frequency required by high-speed machines can be multiple kilohertz (kHz). The high switching frequency capability of WBG devices enables high-speed machines with a larger number of poles, which can reduce the weight and volume. MW-level (>1000 HP), high-speed (10,000-20,000 r/min) motors are used in petroleum refining industries, natural gas infrastructure, and other industrial applications. Deployment of medium-voltage variable speed drives in these MW class motors could provide considerable energy savings of up to 0.7% to 1.8% of the total US electricity consumption [46]. A Si-based electric drive integrated with a standard 60 Hz motor operates at 1800 or 3600 r/min while the compressor runs at 15,000-20,000 r/min. The motor is connected to the compressor through a gearbox to increase the speed. The high frequency operation capability of SiC MOSFETs at medium voltage and MW power level allows the motor to run at the same speed as the compressor [46], which increases the reliability of the system by eliminating the gearbox.

Experimental results for a SiC-based inverter for high-speed PM synchronous machines are presented in [47]. A GaN-based drive for a high-speed single-phase BLDC motor is presented in [48]. The efficiency of the GaN-based motor drive is around 4% higher than a Si-based drive [48]. An overview of how electric turbochargers and superchargers can

improve the thermodynamic efficiency and reduce the size of internal combustion engines is provided in [49], which also reviews various high-speed machines for turbomachinery. The higher switching frequency enabled by a GaN inverter reduces the rotor losses in both slotted and slotless stator type high-speed PM motors [50]. A SiC inverter developed for high-speed PM motors is tested at high switching frequencies up to 500 kHz [51]. The iron loss is the largest component of losses in ultra-high-speed motors, and the switching frequency component causes a large proportion of the total iron loss [52]. A 100,000 r/min, 1.7 kW motor operating at a switching frequency of 120 kHz is able to achieve a maximum total efficiency of 94.3% [52]. As the switching frequency increases, the motor efficiency improves but the inverter efficiency decreases. The efficiency of the combined motor drive system is 91% at a switching frequency of 80 kHz, which is very high for a motor running at 100,000 r/min [52]. The winding temperature decreased from 56 °C to 51 °C when the switching frequency is increased from 40 kHz to 120 kHz [52]. A medium voltage 3-phase two-level converter based on 10 kV/10 A SiC MOSFETs for motor drive applications is presented in [53].

C. *High-Temperature Applications*

The maximum operating temperature of a semiconductor material is determined by its bandgap. Therefore, semiconductors with a wider bandgap can operate at higher temperature. However, to this point, the current unavailability of high temperature packaging has limited the operating temperature of SiC modules to 200 °C [9]. Additionally, SiC has a higher thermal conductivity than Si, allowing SiC devices to dissipate heat produced by losses faster, so SiC devices can operate at much higher power densities than Si devices. Integrated motor drives (IMDs), which involve placing the power electronics with the motor inside the motor housing, are becoming popular in aerospace and automotive applications [54]. In [55], a review of IMDs is provided with special attention given to IMDs in EV traction motor drives. IMDs also offer direct replacement for inefficient direct on-line motors. Close physical integration of the converter and the motor results in a temperature increase in the power electronic components, which has limited power levels to 7.5 kW for Si-based IMDs [54]. WBG devices with their high-temperature capability make IMDs feasible for higher power levels. With integrated systems, the efforts for maintaining electromagnetic compatibility (EMC), the high-voltage harness, and the cooling systems can be reduced significantly. An integrated modular motor drive design using GaN devices is presented in [22].

The development of WBG power modules with reverse-voltage-blocking and high-frequency capability for an IMD using a current-source inverter (CSI) is presented in [56]. An efficiency of 97.7 % is reported for the WBG-based CSI. Meeting the high temperature operation requirement for both passive components and power switches in proximity to the motor where the peak temperature often exceeds 180 °C, is a challenge. Even with the use of film capacitors for the dc link in a VSI-based IMD, the capacitor is bulky and its maximum operating temperature is limited. A CSI topology with WBG power devices operating at a high switching frequency of more than 100 kHz is a promising solution for IMDs because both the dc link inductor and WBG power devices are suited for high temperature operation. A CSI also has less EMI and better fault tolerance with PM machines than a VSI [56].

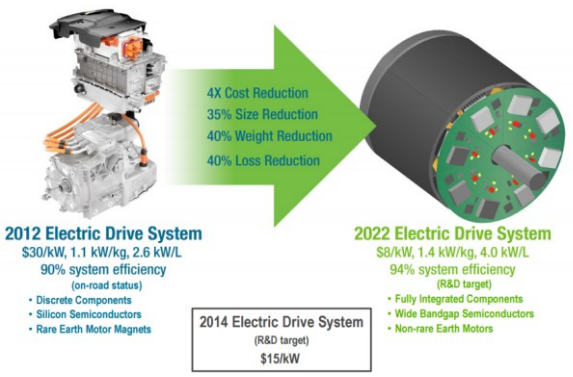

Fig. 2. US DOE 2022 electric drive system target for an electric vehicle [64].

D. *WBG Devices for EVs and HEVs*

Electrification is the most promising solution for environmentally friendly transportation systems [57], [58]. The enabling technologies and solutions for the transportation electrification are discussed in [57]. The continuing trend towards electrification of transportation promises an important role for power electronics [59]. A review of the WBG devices and their adoption in EVs and HEVs is presented in [60]. Table II shows various SiC traction inverter prototypes and some of their important features as reported in literature. For a typical HEV driving cycle, the drivetrain is lightly loaded most of the time [61]. Therefore, the vehicle-level fuel efficiency is substantially reduced by the high losses of Si IGBTs. SiC MOSFETs, which have lower losses, can greatly improve the fuel economy of HEVs [61]. In 2014, Toyota, in collaboration with Denso, introduced a prototype SiC power control unit for its Prius HEV, which demonstrated a 5% improvement in the fuel economy over the standard JC08 Japanese drive cycle [62]. The 2020 traction inverter power density target set by the DOE is 13.4 kW/L and the specific power target is 14.1 kW/kg with a target cost of less than $3.30/kW for quantities of 100,000 units while maintaining a 15-year reliability at ambient operating temperatures from −40 to +140 °C [63]. Fig. 2 shows the 2022 electric drive system target set by the DOE in its advanced power electronics and electric motor research and development program [64]. WBG devices can operate at higher junction temperatures, which allows the use of hotter coolant and smaller thermal management systems and can potentially help facilitate air cooling without sacrificing performance. Various advantages

of WBG devices for electric propulsion are presented in [65]-[69]. SiC modules have been developed for power levels up to 88 kW for automotive inverters using new 900 V SiC MOSFET technology [70], [71]. Cree modeled the efficiency of a 90 kW drive for a Ford Focus car and showed that loss reductions of 65% and 73% in the inverter could be achieved for environmental protection agency city and highway driving cycles, respectively, by using these 900 V SiC MOSFETs instead of Si IGBTs [72]. The higher efficiency of the electric drive will reduce the required weight, volume, and cost of the battery. SiC MOSFETs are capable of synchronous rectification, so no anti-parallel diodes are required. The first 650 V, 420 A enhancement-mode GaN-based power module for the world's most compact 55 kW all-GaN traction inverter is under development [63], [73].

Direct-cooled power module technologies suitable for WBG device-based EV/HEV inverters are presented in [74]. The power module structure has a thick copper heat spreader located beneath the semiconductor chip, which has a 34% lower thermal resistance compared to conventional direct-cooled power modules [74].

In [75], a SiC MOSFET power module design in a segmented two-level inverter with 125 kW peak power and 30 kHz switching frequency is presented. The manifold microchannel heat sink technology for substrate and capacitor cooling helps in achieving maximum thermal performance.

III. Industry Prototypes and Products Review

Table III summarizes industry products and prototypes that use WBG device-based motor drives. In 2014,

Fig. 3. Mitsubishi Electric EV PM motor with built-in SiC inverter [86].

Mitsubishi Electric developed a prototype EV drive system using a PM motor with an integrated SiC inverter that is half the size of a system with external inverters and has less than half the losses of Si-based systems [86]. This motor drive (14.1 L, 60 kW) has improved thermal resistance between the motor drive system and the cooling system and is shown in Fig. 3.

The KSB Group prototyped a 22 kW super-compact high-efficiency synchronous reluctance motor with an integrated inverter using SiC devices in 2017 [87]. This IMD approach, combined with a new cooling system, reduced the volume of the motor drive by over 25% compared with the traditional design.

In 2017, Beckhoff presented a distributed servo drive system employing compact motors with integrated high-efficiency SiC devices, which provides significant savings in cost, space, materials and installation effort [88].

TABLE II
SiC Inverter Prototypes for Traction Applications

Reference and year	Description	Power	Efficiency	Power density	Comments
[76], 2017	EV inverter made of 900 V half bridge modules	200 kVA	Mean 96% and peak 98.1% for Vdc=450 V	-	Inverter driving a 75 HP interior permanent magnet synchronous motor over typical EV driving cycle
[77], 2017	EV inverter 1200 V half bridge modules	110 kVA	Mean 96.3% and peak 98.9%	23.1 kVA/L (17.0kW/L) 16.8 kVA/Kg (12.4 kw/Kg)	140 °C ambient and 105 °C liquid coolant temperature
[78], 2017	Front end boost + 3 phase VSI for EV, 1 kV dc bus	100 kW	-	35 kW/L	PowerAmerica EV inverter development project completed at North Carolina State University
[79], 2018	Megawatt-scale inverter based on a three-level active neutral-point-clamped (3L-ANPC) for hybrid-electric aircraft		99%	12 kVA/Kg	SiC MOSFET for switches operating at carrier frequency and Si IGBT for switches operating at the fundamental frequency; fundamental frequency of 1.4 kHz to drive the high-speed motor unlike the conventional 400 Hz systems
[80], 2018	EV inverter with specially designed 2 in 1 module	128 kW	-	-	Double-sided direct-cooling provides 35% less thermal resistance between the chip and the coolant
[81], 2017	HEV power control unit comprising front end boost and two inverters	430 kVA	-	86 kVA/L	Module with insulated ceramic substrate results in 43% less thermal resistance; passive components directly connected to heat sink using an Aluminum chassis to provide better heat dissipation
[82], 2018	EV inverter	60 kW	-	34 kW/L	140 °C ambient and 65 °C liquid coolant temperature
[83], 2016	Front end boost + VSI for EV	55 kW	99% peak	12.1 kW/L	PCB-based bus bar and planar inverter design
[84], 2018	EV inverter	30 kW	99.5% peak	15 kW/L	Input dc bus of 250-800 V
[85], 2018	3-level T-type traction inverter	250 kW	98% peak	-	Heavy duty off-road vehicle applications

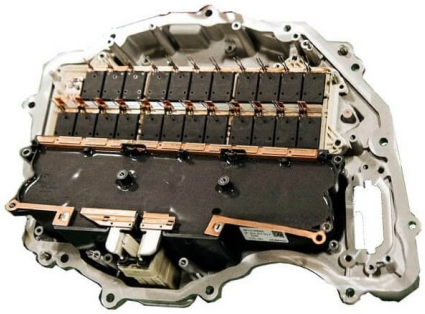

Fig. 4. Tesla Model 3 main inverter, featuring 24 SiC MOSFET modules from ST Microelectronics [91].

John Deere developed a 200 kW SiC dual inverter with a 1050 V dc bus voltage for heavy-duty off-highway and on-highway vehicles working on a PowerAmerica project [89]. The inverter has a power density of more than 25 kW/L, which is substantially improved from the 17 kW/L power density achieved with Si. This significant increase in the power density results from reducing the dc bus capacitance value to 300-400 uF from 1500 uF for the Si based converter, due to the increase of switching frequency from 8 kHz to 15 kHz. The high junction temperature capability and low losses make it possible to use the engine coolant itself for cooling of the power converter in a HEV.

Calnetix Technology has been developing a medium-voltage, 1.6 MW integrated SiC inverter and a high-speed motor running at 15000 r/min for gas compression since 2017 [90]. The targets for this drive are nearly 10 times the power density of a Si-based drive and a 94% net system efficiency without the use of any gears. This integrated drive is well suited for high-speed direct-drive equipment in many industrial sectors like gas compression applications in natural gas pipelines and offshore platforms, air compression for air separation, flywheel-based energy storage, and various power generation and turbo expansion applications.

In 2018, Tesla unveiled an electric drivetrain using 650 V, 100A SiC MOSFETs, as show in Fig. 4, for its Model 3 car [91]. The modules are molded modules using copper ribbon-bonding for MOSFET connections.

Siemens developed a very high power density SiC inverter with micro channel cooling plate for electric and hybrid-electric aircraft. The power electronics of the 104 kVA inverter fit in a box of 1.85 inches×3.7 inches×5.55 inches and weigh only 1.98 pounds [92].

IV. Technical Challenges in Realizing The Full Potential of WBG Devices in Motor Drives

To justify the higher cost of WBG devices and fully realize their potential, they must be switched at high speeds, but high switching speeds result in additional EMI generation. High *dv/dt* excites the capacitive coupling paths in the converter, cables, and motor causing substantial CM current to flow and can damage motor insulation. If WBG devices are switched at significantly lower speeds, this will maintain compatibility with present motor winding insulation standards and allow the use of EMI mitigation measures similar to those employed with present IGBT-based drives. However, using a lower switching speed fails to reap the full power density and efficiency benefits from using WBG devices, and these benefits are important to offset the increased cost of WBG devices.

TABLE III
Industry Products and Prototypes Using WBG Device-based Motor Drives

Reference and year	Description	Advantage	Power
[86], 2014	Integrated SiC PM motor drive by Mitsubishi Motors	Half the size and half the losses compared to a Si-based drive	60 kW
[87], 2017	Integrated synchronous reluctance motor drive by KSB Group	Super compact, high efficiency and 25% reduction in volume compared to a Si-based drive	22 kW
[88], 2017	Integrated SiC distributed servo drive by Beckhoff	Significant savings in cost, space, material and installation efforts	0.61-1.78 kW
[89], 2018	SiC inverters for vehicles with 1050 V dc bus voltage by John Deere	Power density of 25 kW/L vs 17 kW/L for Si-based drive; Cooling possible with engine coolant	200 kW
[90], 2017	Medium-voltage 1.6 MW integrated SiC high-speed PM motor drive by Calnetix (Ongoing)	94% efficiency, 3-4% more efficiency, 10 times power density compared to a Si-based drive and compact footprint of 3.1 m^2/MW	1.6 MW
[91], 2018	SiC EV inverter for Model 3 by Tesla	Efficiency and high power density	200 kW
[92], 2018	SiC inverter for hybrid and full electric aircraft by Siemens	Efficiency and high power density	104 kVA

A. Trade-off Between High Switching Frequency and EMI

If a high switching frequency is used, as required for low-inductance motors and high-speed motors, the conducted emissions increase significantly and an EMI mitigation strategy must be implemented to comply with EMC standards. IEC standard 61800-3 describes the EMC test requirements and test methods for adjustable speed electric drives. In [93], the direct relation between rise/fall time of a trapezoidal switching waveform of a power device and its high-frequency spectral amplitude is discussed. High switching speeds result in higher EMI generation. The increase in the conducted CM EMI of a WBG device-based PWM inverter-based motor is investigated and quantified in [94]. The influence of *dv/dt* on the conducted CM EMI is generally limited while the influence of switching frequency is more significant [94].The comparison of CM EMI with Si IGBT based drive is shown in Fig. 5 [94].

In [95], the conducted EMI performance in SiC JFET and Si IGBT based motor drives has been compared. The excited parasitic oscillations during switching transients are higher in

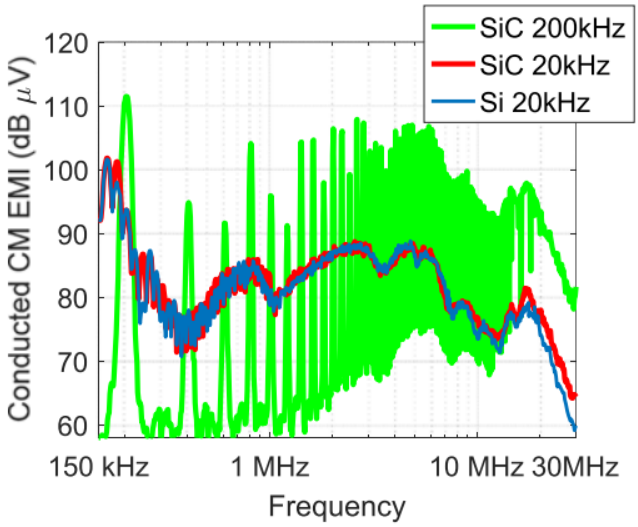

Fig. 5. Comparison between the CM EMI of Si IGBT- and SiC MOSFET-based motor drives [94].

the SiC JFET inverter, which is the main cause of the different noise performance between the two motor drives. The higher switching speed of SiC devices results in higher current overshoots and parasitic oscillations, especially in conducted differential mode EMI over the frequencies between 3 and 15 MHz, as shown in Fig. 6. The conducted emission caused due to the capacitive coupling of the device terminal with the insulated metal substrate or heat sink in a SiC JFET inverter is investigated in [96], [97]. There is a trade-off between switching loss and EMI generation. The high switching speed causes a 20–30 dB increase in the high-frequency spectral content of the switching waveform and a fivefold increase in the *dv/dt* at the inverter output [98]. The high switching frequency increases the CM emissions substantially and makes the CM choke design more challenging. In [99], a CM choke designed to comply with EMC standards for a SiC device-based motor drive operating at 200 kHz is found to be significantly larger and heavier than a CM choke designed for 20 kHz operation.

Fig. 7 shows the comparison of CM EMI of a SiC-based motor drive at 20 kHz and 200 kHz. Considering this, innovative filter topologies and CM voltage cancellation techniques should be adopted for high frequency operation of a WBG device-based drive. A new concept of the balanced inverter topology and dual-winding stator configuration for CM voltage cancellation for PWM motor drives, as shown in Fig. 8, is introduced in [100]. Two complementary CM voltages generated with the balanced inverter topology and a symmetrical circuit with dual-winding stator configuration cause the CM voltages to get canceled in the windings. Table IV reports the solutions proposed in various papers to minimize EMI.

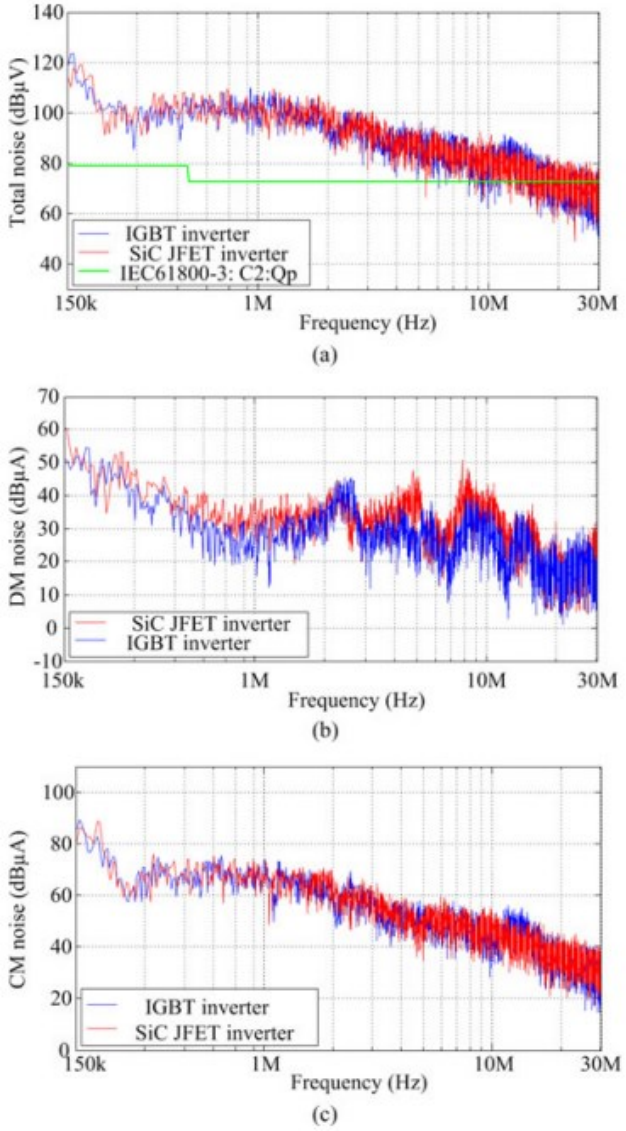

Fig. 6. Comparison of measured EMI spectra without any filter: (a) total, (b) differential mode, and (c) common mode. [95].

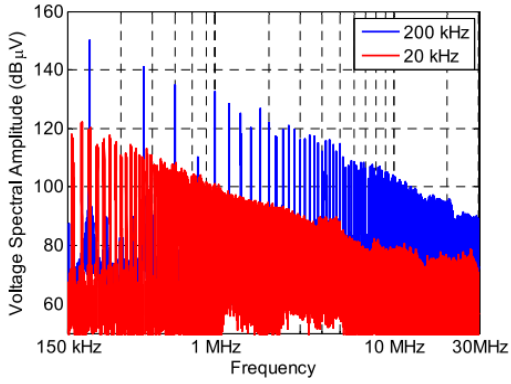

Fig. 7. Comparison of common mode voltage for 200 kHz and 20 kHz for SiC MOSFET based motor drive [99].

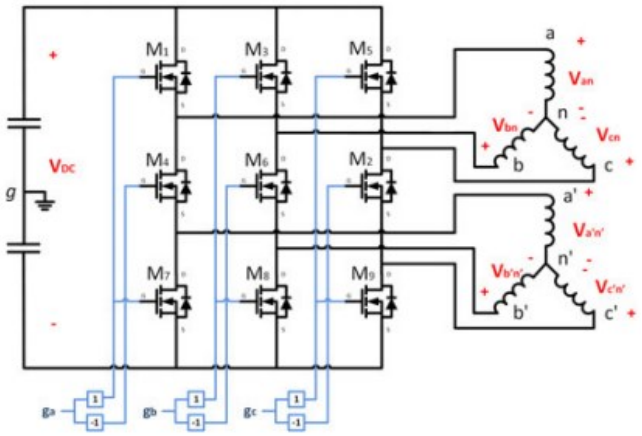

Fig. 8. Balanced inverter topology with dual-winding stator configuration for CM voltage cancellation [100].

B. *Insulation and Bearing Damage Due to High dv/dt*

In motor drives, especially those with long cables between the motor and the drive, the high *dv/dt* created by PWM VSIs creates high voltage stress in the motor insulation due to voltage reflection [108]. A series of high frequency pulses can cause partial discharge in the motor windings, which can lead to premature failure of the interturn insulation in PWM VSI-fed motors. If the voltage generated by a PWM VSI at the motor terminals has a steep front, the voltage distribution among the coils of a winding and among the turns of a coil is highly non-uniform [109]. The amplitude and rise time of the voltage at the machine terminals depends on the length of the cable connecting the motor and inverter, the machine surge impedance and the presence of any filters that increase the rise time.

Bearing currents are caused by the high *dv/dt* of WBG devices and CM voltage, and these bearing currents can reduce bearing lifespans. Magnetic bearings, shaft-grounding brushes, and insulated bearings are known methods to prevent bearing damage due to the high *dv/dt* of WBG devices. In [110], an electromagnetic shielding slot wedge is used to decrease the bearing currents by reducing the capacitive coupling between the stator windings and the rotor. This method is claimed to be more economical and reliable than using shaft-grounding brushes or insulated bearings to prevent bearing damage due to CM currents.

A *dv/dt* filter placed between the drive and the motor can be used to reduce the *dv/dt* at the motor terminals. In [111], *dv/dt* filter and sine wave filter options are compared for preventing high *dv/dt*, and the *dv/dt* filter option results in a higher system efficiency. In [108], a low-loss "RL-plus-C" passive filter for overvoltage suppression and new filters for bearing current mitigation are proposed. These have simple structure, low cost, and, unlike conventional filters, a low power dissipation. A new *dv/dt* filter suitable for use with high power ac motor drives with cable lengths of up to 300 m is proposed in [112], which also has a built-in resistor failure detection circuit. In [113], a novel inductor-less *dv/dt* filter is presented for

TABLE IV
SOLUTIONS TO MINIMIZE EMI

Reference	Solutions and contribution
[95]	1. Ferrite bead positioned on the dc bus between the filter and inverter 2. Ferrite beads between inverter output and motor to suppress CM oscillations
[97]	1. Separated heat sinks to minimize capacitive couplings to reduce CM noise 2. Heat sink of high side switch grounded to improve CM EMI performance 3. RC snubber circuits and ferrite beads to damp parasitic oscillations for better DM EMI performance
[100]	Realization of balanced inverter topology and dual winding stator configuration for CM voltage cancellation
[101]	Digital filters to suppress sampling noise caused by EMI
[102]	Advanced random PWM technique (10 dB attenuation of noise) and EMI filters
[103]	Design of 4-leg GaN inverter to reduce CM voltage
[104]	Comprehensive design procedure for CM filter to suppress conducted EMI
[105]	Novel floated inverter topology for CM EMI reduction
[106]	Dual-VSI fed open end winding motor drive for shaft voltage and ground current suppression
[107]	Performance comparison of floated, balanced inverter with dual stator winding configuration, and 4-leg inverter topologies for CM reduction

100 kW to 1 MW SiC-based VSI. The filter uses the stray inductance between the power device and the VSI output as a filter component instead of a lossy, heavy, and costly filter inductor, with an additional small RC-link. Experimental results using a 1700 V, 300 A SiC MOSFET show that the *dv/dt* at the converter output is limited to 7.5 kV/μs even though the SiC MOSFET was switching at 47 kV/μs. New *dv/dt*-control methods based on adding a drain-gate capacitor to slow down the switching speed for the SiC JFET/Si MOSFET cascade are presented in [114]. A *dv/dt* filter allows the inverter to switch at high *dv/dt* to minimize switching losses while avoiding the problems associated with high *dv/dt* in the motor and cable [113]. Thus, the *dv/dt* filter reduces the common mode noise generated due to parasitic capacitances inside the motor [110]. If there is a cable between motor and inverter, the *dv/dt* filter is placed near the inverter so that it will also reduce the common mode noise generated due to the parasitic capacitance of the cable [99]. Additionally, the reduced *dv/dt* at the motor terminals reduces the stress on the motor insulation [108].

C. *Packaging Challenges for High Voltage and High Temperature Devices*

Traditional power module packaging technology has some limitations when trying to build high-voltage and high-temperature modules for WBG devices. The coefficient of thermal expansion mismatch between base plates and the substrate, solder void formation in the die attachment and the direct bond copper to base plate bond, and parasitic effects caused by wire bonds are some of the challenges [115]-[121]. Designing and manufacturing new compact high voltage SiC-based power modules requires important consideration regarding insulation materials, design of creepage and

TABLE V
GATE DRIVER DESIGN

Content	References
Overall design	[24], [25], [122], [123]
Resonant gate driver	[124], [133]
Parasitic elements in gate-source loop	[28], [29], [125]
Miller effect/ crosstalk	[126]-[129], [138], [139]
Overshoot and oscillations in presence of parasitic elements in layout or load	[130], [131]
Active gate driver	[23], [130]- [132]
High temperature gate driver	[134]- [136]

clearance, an optimized layout design to minimize parasitic inductances, and suitable external bus bar connections. Wolfspeed designed and tested 10 kV/40 A SiC MOSFET and 24 kV/30 A SiC IGBT power modules designed for 200 °C operation [9]. The module housing is made of a high temperature plastic designed to meet UL and IEC creepage requirements based on 15 kV operation. A high temperature Silicone gel is used to provide internal clearances. Clamped inductive load test results presented for the module at 8 kV/28 A show switching speeds up to 111 kV/μs, which is 10 times better than the conventional Si IGBTs. Wolfspeed developed an evaluation module with a compact footprint using 24 kV SiC IGBTs under a contract with the U.S. Army Research Lab [9]. The module was designed to operate in a dielectric fluid as the terminal spacings do not meet clearance requirement to withstand breakdown in open air. Clamped inductive load testing performed at 14 kV/22 A demonstrates a switching speed of 46 kV/μs, with some degradation observed around 125°C. However, this device and its performance are expected to improve substantially with further development.

V. CONVERTER DESIGN CONSIDERATIONS USING WBG DEVICES

Because of the faster switching and unique characteristics of WBG devices, common design practices for Si-based converters may not extract the best performance from WBG devices. This section covers the important considerations for WBG device-based converter design. The discussion is focused on SiC MOSFETs and enhancement mode GaN high electron mobility transistors (HEMTs), because they are currently the most popular WBG devices for motor drive applications [64], [73], [89]-[92].

A. Gate Driver Design

To achieve their full efficiency benefits, it is crucial to drive SiC MOSFETs in a way that minimizes conduction and switching losses [122]. Fig. 9 shows the typical features of an advanced gate driver integrated circuit (IC). The IC has separate turn-on and turn-off paths, and a negative voltage can be applied during turn-off. Active Miller clamping allows the driver circuit to sink the Miller current across a low impedance path to prevent spurious turn-on. Desaturation protection guards the switching device during a short-circuit event by detecting the the drain-source voltage of the device. When the voltage at the DESAT pin exceeds a certain threshold, the output of the IC is driven low. A programmable

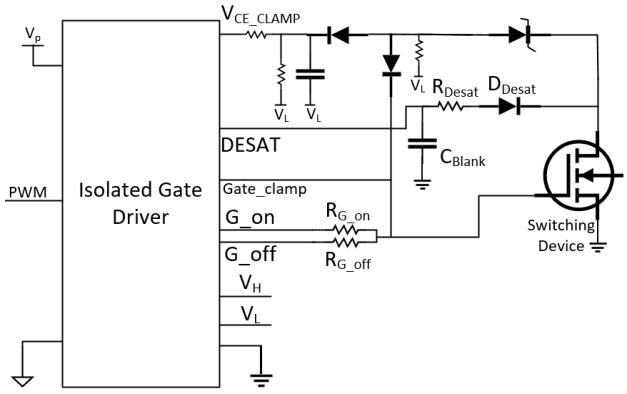

Fig. 9. Important features of an advanced gate driver IC.

blanking time is allowed to prevent false alarms during the switching transition. Many gate driver ICs also have a soft turn-off feature to prevent large drain-source voltage overshoots when the device is turned off after a short-circuit event. This is crucial because a large voltage overshoot can damage the device.

The gate driver design considerations and challenges for high power SiC MOSFETs are presented in [123]. Table V summarizes the literature on various aspects of gate driver design for WBG devices. A good gate driver must decrease the switching power losses, have protection features, and be electromagnetically compatible. In [24], an overview and a comparative study of the state-of-the-art gate driving mechanisms for SiC MOSFETs are presented. A high-speed gate driver has been developed and optimized for a commercially available SiC MOSFET power module in [25].

The main aspects influencing switching behavior are the dependence of the turn-on and turn-off energy of the SiC MOSFET on the gate resistance, gate drive current requirements, and Miller effect [123]. The peak gate current available during the switching transient is critical in achieving rapid switching transitions [123], [124]. Preventing gate voltage overshoot and ringing following a switching transition is necessary to ensure reliability of the gate insulation [124]. As shown in Fig. 11, Lp4 and Lp6 represent the common source inductance and Lg1+Lp4 and Lg2+Lp6 represent the parasitic inductance of the gate-source loop. The parasitic inductance of the gate-source loop needs to be minimized because there is a trade-off between the gate voltage overshoot and switching speed [124]. A resonant gate driver to reduce the switching losses is proposed in [124], which enables the removal of the gate resistor by absorbing the parasitic inductance in the gate path. In [28], equivalent circuit models incorporating all of the parasitic elements are developed for the switching of a SiC MOSFET. These circuits can be used to design the snubber or damping circuits to prevent undesirable oscillations during switching. An analytical treatment of self-sustained oscillations in WBG device based circuits is provided in [29]. In [125], switching behavior of a SiC MOSFET regulated by a gate driver is modeled, and mechanisms for suppressing the ringing and overshoot are discussed.

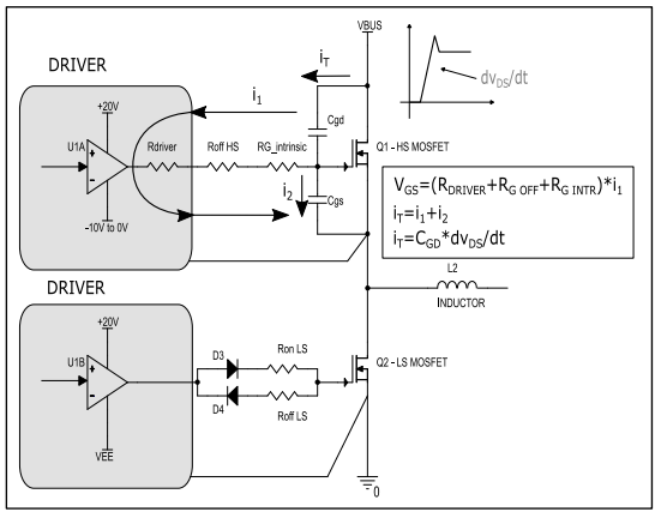

Fig. 10. Miller turn-on phenomenon [122].

The gate driver IC used to drive the high side switch in a half-bridge configuration must have a high CM transient immunity (CMTI). CMTI is defined as the maximum slew rate of the voltage between two isolated grounds. Insufficient CMTI can cause malfunction of the gate driver. The CM current injection in the control circuit through the coupling capacitor of an isolated power supply or through the parasitic capacitance of the isolation in gate driver IC can corrupt control signals on the primary side. Isolated power supplies with coupling capacitance as low as a few pF are available, which ensures high *dv/dt* noise immunity. The CM current can be minimized by using a CM choke if the coupling capacitor is not small [11].

SiC MOSFETs and GaN HEMTs have relatively low gate-source threshold voltages of around 2.5 V and 1.3 V, respectively, which decrease with the junction temperature [126]. These low threshold voltages make them more immune to *dv/dt* noise [127]. Therefore, it is crucial to design the gate driver circuit with low impedance. The fast switching can cause high *dv/dt,* which causes displacement current to flow through the Miller capacitance of the power switch and can lead to an unintended dynamic turn-on of the switch in the off-state in a half-bridge configuration [127]. This is called the Miller effect or crosstalk and is depicted in Fig. 10. A Miller clamp circuit can sink the Miller current across a low impedance path in a high *dv/dt* situation. If the gate driver IC does not have an active Miller clamp feature, an optimum ratio of turn-on and turn-off path resistances and the use of a negative supply voltage during turn-off can provide protection against spurious turn-on. A specific mathematical analysis of the crosstalk phenomenon is provided in [127]. In [128], a new gate driver circuit for SiC MOSFETs designed to attenuate the negative voltage spikes due to Miller effect in a half-bridge configuration is presented. An intelligent gate driver that actively controls the gate voltages and impedances

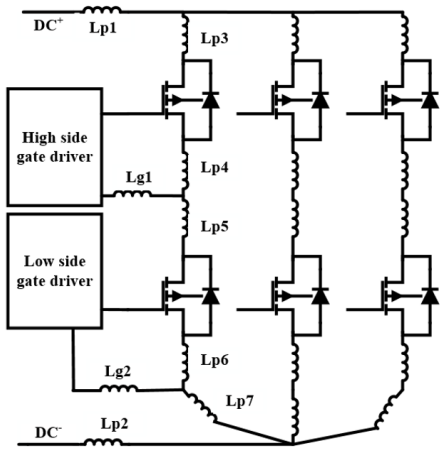

Fig. 11. Parasitic inductances of the commutation and gate-source loops.

of the gate loop of both devices to suppress crosstalk in a phase-leg configuration during switching transients is presented in [129].

The high *di/dt* and *dv/dt* in WBG devices can cause very high voltage overshoot and oscillations due to the presence of parasitic inductance in the layout and any parasitic capacitance in the load [130], [131]. An active gate driver (AGD) is proposed in [130] for SiC MOSFETs, which controls the *di/dt* and *dv/dt* of the device by using appropriate gate resistances during switching transients. An inductive-resistive (*L-R*) filter is connected between the inverter and the induction motor (IM) to decouple the interwinding capacitance of the motor from the device [130]. Both the AGD with an *L-R* filter and a modified two-stage active gate driving technique without an *L-R* filter achieve 50% reduction in device current overshoot while driving an IM.

A programmable high-bandwidth gate driver for GaN that can shape GaN switching during the transient by activating a desired sequence of output resistances is demonstrated in [132]. This can provide low switching loss while reducing overshoot, oscillation, and EMI. A new resonant gate driver circuit is proposed in [133] that achieves 50% reduction in power taken from the gate supply by recycling the energy wasted in the gate resistance of the conventional gate driver circuit. This power saving is significant, especially at high switching frequencies.

To take advantage of the high temperature capability of WBG devices, high temperature gate drivers rated at 180–200 ℃ are presented in [134]-[136]. The characteristics, commercial status of GaN power devices, and challenges encountered in GaN-based converter design are reviewed in [36].

A multi-stage gate driver based on a switched resistor topology that can reduce the drain-source peak voltage by 45% while maintaining equal turn-off losses for SiC MOSFETs is presented in [137].

TABLE VI
POWER CIRCUIT DESIGN

Content	References
Complete converter design	[34], [144], [145]
Stray inductance of power module	[142], [143]
Bus bar design	[34], [143]
DC link capacitance selection	[22], [34]
Power loop design for GaN HEMT	[146], [147]

Two simple, efficient, and cost-effective gate assist circuits to actively suppress the crosstalk utilizing the intrinsic properties of SiC power devices are presented in [138]. The first gate assist circuit reduces the gate loop impedance to mitigate crosstalk, and the second gate assist circuit actively controls the gate voltage for crosstalk elimination.

A novel gate driver with two additional capacitors to create a low turn-off gate impedance to suppress the crosstalk is presented in [139]. The two capacitors enable decoupling the common source parasitic inductance from the gate-source loop and bypassing the Miller current.

A novel open-loop gate control of the turn-on transient for SiC MOSFETs for hard switching applications is presented in [140]. It can reduce the EMI caused due to the high turn-on speed in a half-bridge configuration while achieving low turn-on losses. The controller is of low cost and has a simple structure. The *di/dt* and *dv/dt* of the device are controlled independently by controlling the gate-source voltage profile during the current rise phase and the gate current during the voltage falling phase.

A minimal footprint gate driver with low input CM current, and a short circuit protection scheme is designed in [141] for medium voltage SiC devices that are exposed to a high voltage stress and a very high *dv/dt* (10 kV/ μs to 100 kV/ μs). The gate driver isolation stage has an ultra-low coupling capacitance of approximately 2 pF and is able to withstand the high isolation voltage. A ground shield added to the primary winding further reduces the effective capacitance to around 1.2 pF.

B. Power Circuit Design

As shown in Fig. 11, the inductances Lp3 to Lp7 constitute the stray inductances of the power module and are optimized by the manufacturer. If discrete devices are used, then it is the responsibility of the circuit designer to minimize the interconnection inductances of the devices. Stray inductances in the dc side of the loop, Lp1 and Lp2, should be minimized to reduce the commutation loop inductance. The Lp1 and Lp2 inductances can be minimized using the dc bus bar, the dc link capacitors, and high frequency decoupling ceramic capacitors with minimum equivalent series inductance (ESL).

Table VI summarizes the main papers addressing different aspects of converter design using WBG devices. Minimizing the parasitic inductance of the commutation loop is crucial because the parasitic inductance causes voltage overshoot during the device turn-off. There is a tradeoff between the voltage overshoot and the achievable *di/dt* because the voltage overshoot should not exceed the rated voltage of the device. The stray inductances of the power module, the dc bus bar, the dc link capacitors, and the high-frequency decoupling capacitors constitute the commutation loop inductance [34].

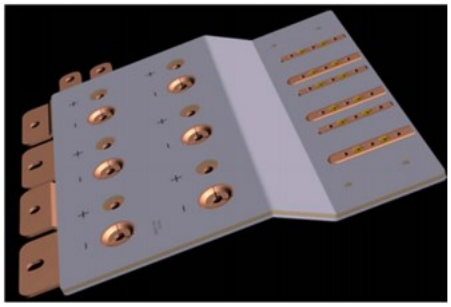

Fig. 12. The dc laminated bus structure for Wolfspeed's 250 kW traction inverter [34].

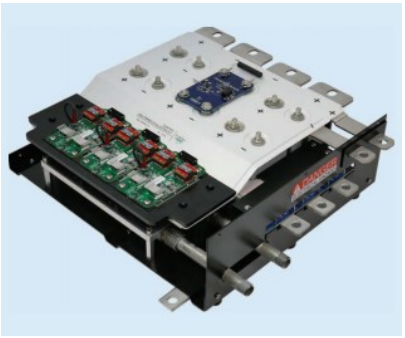

Fig. 13. A compact 16 kg, 250 kW SiC-based three-phase inverter by Wolfspeed [34].

Commercialized SiC MOSFET modules generally have a stray inductance around 10-15 nH, and some designs achieve an inductance as low as 5 nH [142]. A SiC power block based on General Electric's 1.7 kV/480 A SiC MOSFET module has a 4.5 nH loop inductance [143]. A laminated bus bar structure was designed with 12 dies with 1.7 kV/40 A ratings connected in parallel, significantly reducing the parasitic inductance. In traditional modules with similar ratings, the wire bonds and traces are routed in the direct-bonded copper, which results in loop inductances around 10-15 nH [143].

Specially designed dc laminated bus bars are used to minimize the parasitic inductance [34]. An example of low stray inductance dc bus bars for a 250 kW SiC inverter is shown in Fig. 12 and the developed SiC inverter is shown in Fig. 13. The multiphysics-based design of a dc bus bar is presented in [34], which can result in low equivalent series resistance (ESR) and ESL. The design of the terminals connecting the power module and the dc bus bar is also critical as it affects the inductance [34], [143]. The complete SiC MOSFET based converter design with dc bus bars, gate driver, dc link capacitor bank and thermal management is discussed in some papers [11], [34], [143]-[145].

In general, electrolytic, metallized polypropylene, or ceramic capacitors are used in power electronics applications. Cost, voltage blocking capability as a function of temperature, capacitance stability as a function of temperature and voltage, and thermal resistance from hot-spots to the case each influence the selection of the optimal dc-link capacitor [34]. Film capacitors have best overall performance except that

TABLE VII
SHORT-CIRCUIT CAPABILITY AND PROTECTION OF WBG DEVICES

Content	References
Investigation of short-circuit capability of SiC	[149]-[151], [154]-[159]
Investigation of short-circuit capability of GaN	[161]-[163]
Fast short-circuit protection circuits	[152], [153], [160], [164]

their capacitance per unit volume is small [34]. For electrolytic capacitors, the limiting factor for the dc link capacitance is the RMS current ripple requirement because electrolytic capacitors have relatively high ESR, requiring the parallel connection of many capacitors [22]. However, for film capacitors, the determining factor is the capacitance required for the voltage ripple requirements because film capacitors have a low ESR [22].

Fig. 14. A 1.7 kV/480 A SiC module with gate driver developed by General Electric [143].

For film capacitors, the required capacitance decreases as the switching frequency increases up to an optimal frequency, beyond which the capacitance cannot be reduced any further due to the RMS current rating requirement. This optimal frequency can be as high as 100 kHz, as simulated in [22]. Thus, the high switching frequencies of WBG devices can result in a smaller dc link capacitance than that required with Si devices, if film capacitors are used.

In [143], a highly integrated power block suitable for low-voltage, high-power applications ranging from hundreds of kilowatts to several megawatts is presented and is shown in Fig. 14. The design process for a 312 kVA, 99.3% efficient SiC MOSFET inverter using ten parallel-connected power modules in each phase leg is presented in [144]. In [145], a 30 kVA SiC inverter has been developed for operation in 180 °C ambient temperature to investigate the challenges of harsh environment power electronics.

A very low-inductance commutation loop design based on a four-layer printed circuit board for GaN HEMT is presented in [146]. In [147], an improved power loop design with a vertical structure is proposed for lateral structure GaN transistors and is tested in a 3-phase motor drive. The influence of parasitic effects like cross conduction and stray inductances in a GaN phase-leg configuration is analyzed in [148].

C. Short-Circuit Capability and Protection of WBG Devices

WBG devices have less capability to withstand short-circuits than Si IGBTs and MOSFETs due to their smaller chip area and higher current density. Table VII reports the main papers available that investigate the short-circuit capability and fast protection circuits for GaN and SiC.

According to [149], for a 1200V/33A SiC MOSFET, device failure occurs after approximately 13 μs during a hard short-circuit fault at a dc link voltage V_{dc} of 600 V. However, a substantial leakage current after 5 μs of the short-circuit condition indicates degradation between gate and source terminals. The temperature dependence of the short-circuit capability of SiC MOSFETs is investigated in [150] by testing up to 200 ℃. The short circuit withstand time of SiC MOSFETs reduces as the current density, case temperature, and dc bus voltage increase [150]. The short-circuit ruggedness of SiC MOSFETs is investigated, and two different failure phenomena are reported in [151]. Three overcurrent protection methods, capable of clearing a short-circuit fault within 200 ns, are presented in [152]. In [153], a fast short-circuit detection and protection is recommended after analysis of the short-circuit behavior of a SiC MOSFET. The fastest detection speed was 180 ns, and the experimental results show that the drivers can clear a short-circuit fault within 420 ns for SiC MOSFET.

1200 V SiC MOSFETs pass one hundred 10 µs short-circuit events at 600V dc bus voltage, and 3300V MOSFETs pass 5 microsecond short-circuit event at 2200V bus voltage [154]. The short-circuit causes an almost reversible positive threshold voltage shift. A dynamic electro-thermal simulation in Saber and analysis approach for designing the device and characterizing the short-circuit safe-operating-area is presented in [155]. The model can simulate the failure time and junction temperature at failure for different gate-source voltages and drain-source voltages. The results presented in [156] demonstrate that SiC MOSFETs are relatively robust to single short-circuit events up to about half of their rated voltage. For higher voltages, the device fails in less than 10 µs. The required short-circuit withstand time is generally 10 µs with conventional protection techniques.

A gate driver with a soft turn-off feature during turn-off under short-circuit conditions is developed in [157]. The 1200 V modules failed under short-circuit tests at 860 V in about 2 µs to 3 µs [157]. It is concluded that the non-uniform stress distribution caused by parameter mismatch among the chips of multichip modules adversely impacts the short-circuit capability. Multiple devices with different gate-source threshold voltages were connected in parallel and it was found that the device with the lowest threshold voltages initiated the failure [157].

A 10 kV SiC MOSFET is safely turned off by a protection circuit with 1.5 µs response time at 6 kV dc link voltage during a hard short-circuit [158]. The degradation of the gate oxide is caused by the heating during the short-circuit, and thermal management of the gate oxide can increase the short-circuit capability of the SiC MOSFETs [159].

A fast and cost-effective protection circuit for SiC MOSFETs during hard short-circuits with a detection time less than 1 µs is presented in [160]. It detects hard short-circuits with high noise-tolerance by monitoring both the gate-source

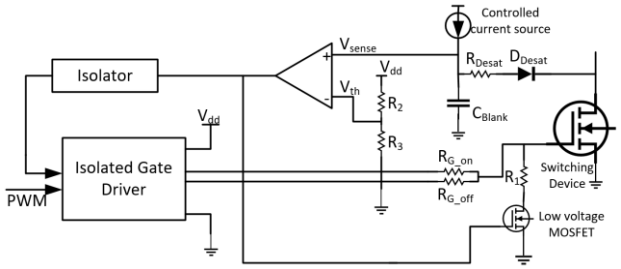

Fig. 15. An ultrafast short-circuit protection circuit for GaN HEMTs [164].

voltage and the gate charge during a turn-on transient because there is a substantial difference in gate charge characteristics during hard short-circuits and normal turn-on operation. High noise-tolerance of the protection circuit is very important in WBG device-based circuits. It does not require a blanking time and the reference gate-source voltage can be set to the Miller plateau voltage. Therefore, it is faster than conventional protection circuits and is suitable for SiC devices [160].

Short-circuit capability tests and degradation tests were performed for analyzing the short-circuit robustness of 650 V enhancement mode GaN HEMTs in [161]. Devices were robust during the 10 μs short-circuit for V_{dc} lower than 350 V and failure was reported at V_{dc} higher than 375 V within hundreds of nanoseconds. Similar failure behavior was observed in [162] and [163]. The recommended short-circuit protection response time for enhancement mode GaN HEMT must be around 200 ns [161]-[163].

The response time of desaturation protection for most of the commercially available gate driver ICs is not fast enough to protect a SiC or GaN device. An ultrafast short-circuit protection circuit for GaN HEMTs, as shown in Fig. 15, is presented in [164] that has a response time of 210 ns. The drain-source voltage is sensed and compared to a threshold value similar to a conventional desaturation protection. The soft turn-off after a short-circuit is implemented using a low voltage MOSFET that is turned on by the fault signal and creates a voltage divider with R_{G_on} and R_1. A lower gate voltage limits the saturation current and thus prevents large voltage overshoot on the gate-source terminals of the device during turn-off.

D. Reliability of WBG Devices

Si MOSFETs and IGBTs are generally tested according to Joint Electron Device Engineering Council (JEDEC) standards. Testing for Si MOSFETs typically includes high-temperature gate bias (HTGB), high-temperature reverse bias (HTRB), high temperature storage (HTS), high temperature high humidity reverse bias (H3TRB), temperature cycling (TC), and moisture sensitivity level (MSL). In addition to these conventional tests, the unique failure mechanisms of WBG devices must be addressed and a suitable qualification process needs to be developed [165]-[167]. Threshold voltage stability, gate-oxide reliability, reliability of the body-diode, and radiation effects are potential reliability issues for SiC MOSFETs [168]. One of the main challenges for WBG devices is accelerated lifetime testing because insufficient field reliability experience is available to validate the accelerated lifetime models.

The degradation mechanisms and intrinsic reliability performance of SiC devices are reviewed in [169]. The presented field data of over 2 trillion device field hours demonstrate less than 5 failures per billion device hours for commercial SiC MOSFETs. Quantitative reliability measurements and accelerated life data for 900 V SiC MOSFETs for automotive and industrial applications are presented in [170]. These SiC MOSFETs passed all die qualification tests like HTRB, HTGB, thermal shock, and H3TRB [170]. Wolfspeed's E-series SiC MOSFETs passed high-humidity and Automotive Electronics Council (AEC)-Q101 qualification tests and have more than 10 billion field hours [171].

In [172], the reliability assessments for 1.2 kV SiC MOSFETs rated for 200 ℃ junction temperature (T_j) were performed in accordance with AEC-Q101. The HTGB method is usually employed to monitor the variations of gate-source threshold voltage and on-state resistance of MOSFET devices. SiC MOSFETs have stable parameters and good performance over wide temperature ranges from T_j=25 ℃ to T_j=200 ℃ [172].

An overview of reliability and failure analysis in GaN HEMTs is provided in [173], and results on the gradual and catastrophic degradation are presented. A stable high-temperature dynamic on-resistance is the key to the reliability of WBG power devices. ON Semiconductor has developed cascode GaN power devices that show robust performance and reliability [174].

Efficient Power Conversion Corporation (EPC) reports data on qualification testing under HTRB, HTGB, H3TRB, TC, HTS, and MSL in [175]. The stability of the devices under stress conditions shows robustness. The mean time to failure exceeds 10 years at maximum operating temperature and at both maximum drain-source and gate-source voltages under both HTRB and HTGB stress tests [176]. A dynamic upward shift of the on-resistance is the most important failure mechanism of GaN transistors under HTRB stress. The on-resistance increases with drain bias, and the device fails when the resistance exceeds the limits specified in the data sheet [176]. Cosmic radiation is a known cause of failure in Si power devices, specifically IGBTs and MOSFETs. The majority carrier GaN HEMT is intrinsically radiation resistant and there is no requirement for derating, which is needed in Si power devices, in automotive applications that are sensitive to radiation [177].

VI. Conclusion

The benefits and technical challenges of using WBG devices in motor drives are reviewed. WBG devices are enabling technologies for many motor drive applications and especially beneficial for low-inductance motors, high-speed motors, and high-temperature applications. Electric drive applications can benefit significantly from WBG devices in terms of power density, dynamic response, and energy efficiency. However, to achieve the maximum benefits from

using WBG devices, the converter must be designed with appropriate gate drivers than can switch quickly with minimal overshoot and losses, with minimal parasitic inductance in the commutation loop, and with fast short-circuit protection for the WBG switches. This paper also gives a review of industry products and prototypes built using WBG devices. The technical challenges in developing high-voltage and high-temperature packages for WBG devices, the problems caused by high *dv/dt* in motor drives, *dv/dt* filters, and the trade-offs between high switching frequency and EMI are discussed. AEC-Q101 qualified SiC and GaN devices are available for automotive applications and further improvement in reliability is expected. The system level benefits and energy savings due to the high efficiency obtained using SiC devices can offset their high cost. WBG devices are key technologies for vehicle electrification and can be expected to make EVs more efficient and economical in the near future.

REFERENCES

[1] J. Millán, P. Godignon, X. Perpiñà, A. Pérez-Tomás and J. Rebollo, "A Survey of Wide Bandgap Power Semiconductor Devices," *IEEE Trans. Power Electron.*, vol. 29, no. 5, pp. 2155-2163, May 2014.

[2] J. W. Palmour *et al*., "Silicon carbide power MOSFETs: Breakthrough performance from 900 V up to 15 kV," in *Proc. 26th Int. Symp. on Power Semicond. Devices & IC's (ISPSD)*, Waikoloa, HI, Jun. 2014, pp. 79-82.

[3] T. P. Chow, I. Omura, M. Higashiwaki, H. Kawarada and V. Pala, "Smart Power Devices and ICs Using GaAs and Wide and Extreme Bandgap Semiconductors," *IEEE Trans. Electron. Devices*, vol. 64, no. 3, pp. 856-873, Mar. 2017.

[4] A. Bindra, "Wide-Bandgap-Based Power Devices: Reshaping the power electronics landscape," *IEEE Power Electron. Mag.*, vol. 2, no. 1, pp. 42-47, Mar. 2015.

[5] "DE-FOA-0001727: Creating Innovative and Reliable Circuits using Inventive Toplologies and Semiconductors (CIRCUITS)," Advanced Research Projects Agency-Energy (ARPA-E), Jan. 9,2017. [Online]. Available: https://arpa-e.energy.gov/?q=arpa-e-programs/circuits.

[6] J. Wang, V. Veliadis, J. Zhang, Y. Alsmadi, P. R. Wilson and M. J. Scott, "IEEE ITRW Working Group Position Paper-System Integration and Application: Silicon Carbide: A Roadmap for Silicon Carbide Adoption in Power Conversion Applications," *IEEE Power Electron. Mag.*, vol. 5, no. 2, pp. 40-44, Jun. 2018.

[7] C. Liu, R. Abdul Khadar and E. Matioli, "Vertical GaN-on-Si MOSFETs With Monolithically Integrated Freewheeling Schottky Barrier Diodes," *IEEE Electron Device Lett.*, vol. 39, no. 7, pp. 1034-1037, Jul. 2018.

[8] D. Johannesson, M. Nawaz, K. Jacobs, S. Norrga and H. P. Nee, "Potential of ultra-high voltage silicon carbide semiconductor devices," in *Proc. IEEE 4th Workshop on Wide Bandgap Power Devices and Appl. (WiPDA)*, Fayetteville, AR, 2016, pp. 253-258.

[9] Brandon Passmore, Chad O'Neal, Wolfspeed "High-Voltage SiC Power Modules for 10-25 kV Applications" [Online]. Available: http://www.powermag.com/pdf/feature_pdf/1461163294_Woifspeed_Feature.pdf.

[10] A. N. Lemmon and R. C. Graves, "Comprehensive Characterization of 10-kV Silicon Carbide Half-Bridge Modules," *IEEE J. Emerg. Sel. Topics Power Electron.*, vol. 4, no. 4, pp. 1462-1473, Dec. 2016.

[11] S. Hazra, S. Madhusoodhanan, G. K. Moghaddam, K. Hatua and S. Bhattacharya, "Design Considerations and Performance Evaluation of 1200-V 100-A SiC MOSFET-Based Two-Level Voltage Source Converter," *IEEE Trans. Ind. Appl*. vol. 52, no. 5, pp. 4257-4268, Sep.-Oct. 2016.

[12] J. Fabre, P. Ladoux and M. Piton, "Characterization and Implementation of Dual-SiC MOSFET Modules for Future Use in Traction Converters," *IEEE Trans. Power Electron.,* vol. 30, no. 8, pp. 4079-4090, Aug. 2015.

[13] H. Wang, J. Wei, R. Xie, C. Liu, G. Tang and K. J. Chen, "Maximizing the Performance of 650-V p-GaN Gate HEMTs: Dynamic RON Characterization and Circuit Design Considerations," *IEEE Trans. Power Electron.*, vol. 32, no. 7, pp. 5539-5549, Jun. 2017.

[14] K. Peng, S. Eskandari and E. Santi, "Characterization and Modeling of a Gallium Nitride Power HEMT," *IEEE Trans. Ind. Appl.*, vol. 52, no. 6, pp. 4965-4975, Nov.-Dec. 2016.

[15] A. Morya, M. Moosavi, M. C. Gardner and H. A. Toliyat, "Applications of Wide Bandgap (WBG) devices in AC electric drives: A technology status review," in *Proc. 2017 IEEE Int. Elec. Mach. and Drives Conf. (IEMDC)*, Miami, FL, 2017, pp. 1-8.

[16] Ayman Mohamed, Fawzi EL-Refaie, Robert Dean King, "Low-inductance, high-efficiency induction machine and method of making same," US Patent 20120126741 A1, May 24, 2012.

[17] D. Gerada, A. Mebarki, N. L. Brown, C. Gerada, A. Cavagnino and A. Boglietti, "High-Speed Electrical Machines: Technologies, Trends, and Developments," *IEEE Trans. Ind. Electron.*, vol. 61, no. 6, pp. 2946-2959, Jun. 2014.

[18] J. Hornberger, A. B. Lostetter, K. J. Olejniczak, T. McNutt, S. M. Lal and A. Mantooth, "Silicon-carbide (SiC) semiconductor power electronics for extreme high-temperature environments," in *Proc. 2004 IEEE Aerosp. Conf. (IEEE Cat. No.04TH8720)*, Big Sky, MT, Mar. 2004, pp. 2538-2555 Vol.4.

[19] B. Wrzecionko, D. Bortis and J. W. Kolar, "A 120 °C Ambient Temperature Forced Air-Cooled Normally-off SiC JFET Automotive Inverter System," *IEEE Trans. Power Electron.*, vol. 29, no. 5, pp. 2345-2358, May 2014.

[20] M. A. Masrur, "Toward Ground Vehicle Electrification in the U.S. Army: An Overview of Recent Activities," *IEEE Electrific. Mag.*, vol. 4, no. 1, pp. 33-45, Mar. 2016.

[21] N. He *et al*., "20 kW Zero-Voltage-Switching SiC-MOSFET Grid Inverter with 300 kHz Switching Frequecny," *IEEE Trans. Power Electron*.

[22] J. Wang, Y. Li and Y. Han, "Integrated Modular Motor Drive Design With GaN Power FETs," *IEEE Trans. Ind. Appl*., vol. 51, no. 4, pp. 3198-3207, Jul.-Aug. 2015.

[23] A. P. Camacho, V. Sala, H. Ghorbani and J. L. R. Martinez, "A Novel Active Gate Driver for Improving SiC MOSFET Switching Trajectory," *IEEE Trans. Ind. Electron*., vol. 64, no. 11, pp. 9032-9042, Nov. 2017.

[24] D. Peftitsis and J. Rabkowski, "Gate and Base Drivers for Silicon Carbide Power Transistors: An Overview," *IEEE Trans. Power Electron*., vol. 31, no. 10, pp. 7194-7213, Oct. 2016.

[25] S. Yin, K. J. Tseng, C. F. Tong and R. Simanjorang, "Design of high-speed gate driver to reduce switching loss and mitigate parasitic effects for SiC MOSFET," *IET Power Electron*., vol. 10, no. 10, pp. 1183-1189, 8 18 2017.

[26] C. DiMarino, J. Wang, R. Burgos and D. Boroyevich, "A high-power-density, high-speed gate driver for a 10 kV SiC MOSFET module," in *Proc. IEEE Elect. Ship Technol. Symp. (ESTS)*, Arlington, VA, 2017, pp. 629-634.

[27] R. Gao, L. Yang, W. Yu and I. Husain, "Gate driver design for a high power density EV/HEV traction drive using silicon carbide MOSFET six-pack power modules," in *Proc. IEEE Energy Convers. Congr. Expo. (ECCE)*, Cincinnati, OH, 2017, pp. 2546-2551.

[28] D. P. Sadik, K. Kostov, J. Colmenares, F. Giezendanner, P. Ranstad and H. P. Nee, "Analysis of Parasitic Elements of SiC Power Modules With Special Emphasis on Reliability Issues," *IEEE J. Emerg. Sel. Topics Power Electron*., vol. 4, no. 3, pp. 988-995, Sep. 2016.

[29] T. Liu, R. Ning, T. T. Y. Wong and Z. J. Shen, "Modeling and Analysis of SiC MOSFET Switching Oscillations," *IEEE J. Emerging Sel. Topics Power Electron*., vol. 4, no. 3, pp. 747-756, Sep. 2016.

[30] M. Ando and K. Wada, "Design of Acceptable Stray Inductance Based on Scaling Method for Power Electronics Circuits," *IEEE J. Emerging Sel. Topics Power Electron*., vol. 5, no. 1, pp. 568-575, Mar. 2017.

[31] A. Lemmon, M. Mazzola, J. Gafford and C. Parker, "Instability in Half-Bridge Circuits Switched With Wide Band-Gap Transistors," *IEEE Trans. Power Electron.*, vol. 29, no. 5, pp. 2380-2392, May 2014.

[32] L. Zhang, P. Liu, A. Q. Huang, S. Guo and R. Yu, "An improved SiC

MOSFET-gate driver integrated power module with ultra low stray inductances," in *Proc. IEEE 5th Workshop on Wide Bandgap Power Devices and Appl. (WiPDA)*, Albuquerque, NM, USA, 2017, pp. 342-345.

[33] N. R. Mehrabadi, I. Cvetkovic, J. Wang, R. Burgos and D. Boroyevich, "Busbar design for SiC-based H-bridge PEBB using 1.7 kV, 400 a SiC MOSFETs operating at 100 kHz," in *Proc. IEEE Energy Convers. Congr. Expo. (ECCE)*, Milwaukee, WI, 2016, pp. 1-7.

[34] A. H. Wijenayake *et al*., "Design of a 250 kW, 1200 V SiC MOSFET-based three-phase inverter by considering a subsystem level design optimization approach," in *Proc. IEEE Energy Convers. Congr. Expo. (ECCE)*, Cincinnati, OH, 2017, pp. 939-946.

[35] J. Colmenares, D. Peftitsis, G. Tolstoy, D. Sadik, H. P. Nee and J. Rabkowski, "High-efficiency three-phase inverter with SiC MOSFET power modules for motor-drive applications," in *Proc. IEEE Energy Convers. Congr. Expo. (ECCE)*, Pittsburgh, PA, 2014, pp. 468-474.

[36] E. A. Jones, F. F. Wang and D. Costinett, "Review of Commercial GaN Power Devices and GaN-Based Converter Design Challenges," *IEEE J. Emerg. Sel. Topics Power Electron.*, vol. 4, no. 3, pp. 707-719, Sep. 2016.

[37] A. Morya and H. A. Toliyat, "Insulation design for Wide Bandgap (WBG) device based voltage source converter fed motors," in *Proc. IEEE 5th Workshop on Wide Bandgap Power Devices and Appl. (WiPDA)*, Albuquerque, NM, 2017, pp. 74-79.

[38] Alex Lidow, David Reusch, Johan Wilhelm Strydom, and Michael de Rooij, *GaN Transistors for Efficient Power Conversion*, 2nd ed., Chichester, United Kingdom, John Wiley & Sons Ltd., Jun. 26, 2014, pp. 39-54.

[39] Y. Li, D. Han, N. Altintas and B. Sarlioglu, "Design of high-speed toroidal winding surface PM machine with SiC-based inverters," in *Proc. XXII Int. Conf. on Elect. Mach. (ICEM),* Lausanne, 2016, pp. 1559-1565.

[40] Thin gap Mortos [Online]. https://www.thingap.com.

[41] Evan Frank, CTO of ThinGap, "Efficient control of low inductance permananet magnet motors", *UCSB IEE Conference 2016* [Online]. Available: http://iee.ucsb.edu/sites/iee.ucsb.edu/files/evan_frank.pdf

[42] Gui-Jia Su and D. J. Adams, "Multilevel dc link inverter for brushless permanent magnet motors with very low inductance," in *proc. 2001 IEEE Ind. Appl. Conf. 36th IAS Annu. Meeting (Cat. No.01CH37248)*, Chicago, IL, USA, 2001, pp. 829-834 vol.2.

[43] J. O. Krah and J. Holtz, "High-performance current regulation and efficient PWM implementation for low-inductance servo motors," *IEEE Trans. Ind. Appl.*, vol. 35, no. 5, pp. 1039-1049, Sep./Oct. 1999.

[44] S. De, M. Rajne, S. Poosapati, C. Patel and K. Gopakumar, "Low-inductance axial flux BLDC motor drive for more electric aircraft," *IET Power Electron*., vol. 5, no. 1, pp. 124-133, Jan. 2012.

[45] F. Luise *et al*., "Design Optimization and Testing of High-Performance Motors: Evaluating a Compromise Between Quality Design Development and Production Costs of a Halbach-Array PM Slotless Motor," *IEEE Ind. Appl. Mag.,* vol. 22, no. 6, pp. 19-32, Nov. 2016.

[46] "DE-FOA-0001208: Next generation electric machines: megawatt class motors," Department of Energy (DOE), Office of Energy Efficiency and Renewable Energy (EERE), [Online]. Available: https://energy.gov/eere/amo/next-generation-electric-machines.

[47] D. Han, Y. Li and B. Sarlioglu, "Analysis of SiC based power electronic inverters for high speed machines," in *Proc. IEEE Appl. Power Electron. Conf. and Expo. (APEC)*, Charlotte, NC, 2015, pp. 304-310.

[48] W. Lee, D. Han and B. Sarlioglu, "GaN-based single phase brushless dc motor drive for high-speed applications," in *Proc. IECON - 40th Annu. Conf. IEEE Ind. Electron. Soc.*, Dallas, TX, 2014, pp. 1499-1505.

[49] W. Lee, E. Schubert, Y. Li, S. Li, D. Bobba and B. Sarlioglu, "Overview of Electric Turbocharger and Supercharger for Downsized Internal Combustion Engines," *IEEE Trans. Transport. Electrific.*, vol. 3, no. 1, pp. 36-47, Mar. 2017.

[50] A. Tüysüz, R. Bosshard and J. W. Kolar, "Performance comparison of a GaN GIT and a Si IGBT for high-speed drive applications," in *Proc. Int. Power Electron. Conf. (IPEC-Hiroshima 2014 - ECCE ASIA),* Hiroshima, 2014, pp. 1904-1911.

[51] M. Novák, J. Novák and O. Sivkov, "An SiC inverter for high speed permanent magnet synchronous machines," in *Proc. IECON - 41st Annu. Conf. of the IEEE Ind. Electron. Soc.*, Yokohama, 2015, pp. 002397-002402.

[52] *Y. Fu et al*., "Investigation of Efficiency Enhancement of an Ultra-High-Speed Bearingless Motor at 100,000 r/min by High Switching Frequency Using SiC-MOSFET" in *Proc. IEEE Energy Convers. Congr. Expo. (ECCE)*, Portland, OR, 2018.

[53] S. Madhusoodhanan, K. Mainali, A. Tripathi, K. Vechalapu and S. Bhattacharya, "Medium voltage (≥ 2.3 kV) high frequency three-phase two-level converter design and demonstration using 10 kV SiC MOSFETs for high speed motor drive applications," in *Proc. IEEE Appl. Power Electron. Conf. Expo. (APEC)*, Long Beach, CA, 2016, pp. 1497-1504.

[54] R. Abebe *et al*., "Integrated motor drives: state of the art and future trends," *IET Elect. Power Appl.*, vol. 10, no. 8, pp. 757-771, Sep. 2016.

[55] T. M. Jahns and H. Dai, "The past, present, and future of power electronics integration technology in motor drives," *CPSS Trans. Power Electron. Appl.*, vol. 2, no. 3, pp. 197-216, Sep. 2017.

[56] H. Dai *et al.,* "Development of high-frequency WBG Power Modules with Reverse-Voltage-Blocking Capability for an Integrated Motor Drive using a Current-Source Inverter" in *Proc. IEEE Energy Convers. Congr. Expo. (ECCE)*, Portland, OR, 2018.

[57] B. Bilgin *et al*., "Making the Case for Electrified Transportation," *IEEE Transactions Trans. Electrific.*, vol. 1, no. 1, pp. 4-17, Jun. 2015.

[58] R. Reisinger and A. Emadi, "Sensible Transportation Electrification : Get rid of inefficient powertrain designs.," *IEEE Electrific. Mag.*, vol. 1, no. 2, pp. 6-12, Dec. 2013.

[59] J. G. Kassakian and T. M. Jahns, "Evolving and Emerging Applications of Power Electronics in Systems," *IEEE J. Emerg. Sel. Topics Power Electron.*, vol. 1, no. 2, pp. 47-58, Jun. 2013.

[60] D. Han, S. Li, W. Lee and B. Sarlioglu, "Adoption of wide bandgap technology in hybrid/electric vehicles-opportunities and challenges," in *Proc. IEEE Transportation Electrific. Conf. Expo (ITEC)*, Chicago, IL, 2017, pp. 561-566.

[61] M. Su, C. Chen, S. Sharma and J. Kikuchi, "Performance and cost considerations for SiC-based HEV traction inverter systems," in *Proc. 3rd Workshop on Wide Bandgap Power Devices and Appl. (WiPDA)* ,Blacksburg, VA, Nov. 2015, pp. 347-350.

[62] Toyota Global Newsroom, "Toyota Develops New Silicon Carbide Power Semiconductor with Higher Efficiency," May, 2014. [Online] Available: http://newsroom.toyota.co.jp/en/detail/2656842.

[63] "US Department of energy (DOE) ,Office of Energy Efficiency and Renewable Energy (EERE), Electric Drives Technology, 2015 Annual Report," [Online] Available: at http://energy.gov/sites/prod/files/2016/03/f30/FY%202015%20Electric%20Drive%20Technologies%20Annual%20Report.pdf on Nov. 27, 2016.

[64] "US Department of energy (DOE) ,Office of energy efficiency and renewable energy (EERE), Vehicle Technology Office (VTO): Overview of the DOE Advanced Power Electronics and Electric Motor (APEEM) R&D Program," [Online] Available: http://energy.gov/sites/prod/files/2014/09/f18/fy_2014_vto_amr_apeem_overview-final_version.pdf on Nov. 30, 2016.

[65] F. Hilpert, K. Brinkfeldt and S. Arenz, "Modular integration of a 1200 v SiC inverter in a commercial vehicle wheel-hub drivetrain," in *Proc. 4th Int. Elect. Drives Prod. Conf. (EDPC)*, Nuremberg, Sept.-Oct. 2014, pp. 1-8.

[66] S. Jahdi, O. Alatise, C. Fisher, L. Ran and P. Mawby, "An Evaluation of Silicon Carbide Unipolar Technologies for Electric Vehicle Drive-Trains," *IEEE J. Emerg. Sel. Topics Power Electron.*, vol. 2, no. 3, pp. 517-528, Sep. 2014.

[67] A. Merkert, J. Müller and A. Mertens, "Component design and implementation of a 60 kW full SiC traction inverter with boost converter," in *Proc. IEEE Energy Convers. Congr. Expo. (ECCE)*, Milwaukee, WI, 2016, pp. 1-8.

[68] C. Chen, M. Su, Z. Xu and X. Lu, "SiC-based automotive traction drives, opportunities and challenges," in *Proc. IEEE 5th Workshop on Wide Bandgap Power Devices and Appl. (WiPDA)*, Albuquerque, NM,

2017, pp. 25-30.

[69] X. Wen, T. Fan, P. Ning and Q. Guo, "Technical approaches towards ultra-high power density SiC inverter in electric vehicle applications," *CES Trans. Elec. Mach. Syst.*, vol. 1, no. 3, pp. 231-237, Sep. 2017.

[70] J. Casady *et al*., "Ultra-low (1.25mΩ) On-Resistance 900V SiC 62mm Half- Bridge Power Modules Using New 10mΩ SiC MOSFETs," in *Proc. PCIM Europe; Int. Exhibition and Conf. Power Electron., Intell. Motion, Renewable Energy and Energy Manage*., Nuremberg, Germany, 2016, pp. 1-8.

[71] V. Pala, G. Wang, B. Hull, S. Allen, J. Casady and J. Palmour, "Record-low 10mOhm SiC MOSFETs in TO-247, rated at 900V," in *Proc. Appl. Power Electron. Conf. and Expo. (APEC)*, Long Beach, CA, Mar. 2016, pp. 979-982.

[72] Jeff Casady et. al, DOE AMR Review: Cree, Inc., EE0006920 "88 Kilowatt Automotive Inverter with New 900 Volt Silicon Carbide MOSFET Technology". Available at "https://www.energy.gov/sites/prod/files/2016/06/f32/edt073_casady_2016_o_web.pdf"

[73] B. Passmore *et al*., "A 650 V/150 A enhancement mode GaN-based half-bridge power module for high frequency power conversion systems," in *Proc. Energy Convers. Congr. Expo. (ECCE)*, Montreal, QC, 2015, pp. 4520-4524.

[74] K. Numakura *et al*., "Direct-cooled power module with a thick Cu heat spreader featuring a stress-suppressed structure for EV/HEV inverters," in *Proc. IEEE Energy Convers. Congr. Expo. (ECCE)*, Milwaukee, WI, 2016, pp. 1-5.

[75] E. Gurpinar *et al*., "SiC MOSFET-Based Power Module Design and Analysis for EV Traction Systems" in *Proc. IEEE Energy Convers. Congr. Expo. (ECCE)*, Portland, OR, 2018.

[76] K. Olejniczak *et al*., "A 200 kVA electric vehicle traction drive inverter having enhanced performance over its entire operating region," in *Proc. IEEE 5th Workshop Wide Bandgap Power Devices and Appl. (WiPDA)*, Albuquerque, NM, 2017, pp. 335-341.

[77] K. Olejniczak *et al*., "A compact 110 kVA, 140°C ambient, 105°C liquid cooled, all-SiC inverter for electric vehicle traction drives," in *Proc. IEEE Appl. Power Electron. Conf. Expo. (APEC)*, Tampa, FL, 2017, pp. 735-742.

[78] PowerAmerica annual report 2017 [Online]. Available: https://www.poweramericainstitute.org/wp-content/uploads/2017/10/PowerAmerica_2017_Annual_Report_ONLINE.pdf

[79] D. Zhang, J. He, D. Pan, "A Megawatt-Scale Medium-Voltage High Efficiency High Power Density "SiC+Si" Hybrid Three-Level ANPC Inverter for Aircraft Hybrid-Electric Propulsion Systems" in *Proc. IEEE Energy Convers. Congr. Expo. (ECCE)*, Portland, OR, 2018.

[80] T. Hirao *et al*., "EV Traction Inverter Employing Double-Sided Direct-Cooling Technology with SiC Power Device," in *Proc. Int. Power Electron. Conf. (IPEC-Niigata-ECCE Asia)*, Niigata, Japan, 2018, pp. 2082-2085.

[81] S. Yano *et al*., "Development of compact power control unit for HEVs," in *Proc. IEEE Energy Convers. Congr. Expo. (ECCE)*, Cincinnati, OH, 2017, pp. 584-588.

[82] C. Zhang *et al*., "A SiC-Based 100 kW High-Power-Density (34 kW/L) Electric Vehicle Traction Inverter" in *Proc. IEEE Energy Convers. Congr. Expo. (ECCE)*, Portland, OR, 2018.

[83] D. Rahman *et al*., "Design methodology for a planarized high power density EV/HEV traction drive using SiC power modules," in *Proc. IEEE Energy Convers. Congr. Expo. (ECCE)*, Milwaukee, WI, 2016, pp. 1-7.

[84] J. Zhu *et al.* "High efficiency SiC traction inverter for electric vehicle applications," in *Proc. IEEE Appl. Power Electron. Conf. Expo. (APEC)*, San Antonio, TX, 2018, pp. 1428-1433.

[85] Z. Wang *et al*., "A Compact 250 kW Silicon Carbide MOSFET based Three-Level Traction Inverter for Heavy Equipment Applications," in *Proc. IEEE Transportation Electrific. Conf. Expo. (ITEC)*, Long Beach, CA, 2018, pp. 1129-1134.

[86] "Mitsubishi Electric Develops EV Motor Drive System with Built-in Silicon Carbide Inverter", Mitsubishi Electric Corporation [Online]. Available:http://www.mitsubishielectric.com/news/2014/pdf/0213-d.pdf

[87] "KSB Motor Prototype Demonstrates Potential" [Online]. Available: https://www.expresswater.in/news/ksb-motor-prototype-demonstrates-potential/

[88] "Servodrive system uses motors with built-in SiC devices", Beckhoff. [Online]. Available: http://drivesncontrols.com/news/fullstory.php/aid/5584/Servodrive_system_uses_motors_with_built-in_SiC_devices.html

[89] "SiC Inverter for Heavy-Duty Vehicles", John Deere, PowerAmerica project[Online]. Available: https://www.poweramericainstitute.org/wp-content/uploads/2017/02/John-Deere.pdf

[90] "Medium Voltage Integrated Drive and Motor", U.S. Department of Energy (DOE), Office of Energy Efficiency and Renewable Energy (EERE),[Online]. Available: https://www.energy.gov/sites/prod/files/2017/03/f34/Medium%20Voltage%20Integrated%20Drive%20and%20Motor_0.pdf

[91] "About the SiC MOSFET Modules in Tesla Model 3" [Online]. Available:"https://www.pntpower.com/tesla-model-3-powered-by-st-microelectronics-sic-mosfets/

[92] "Siemens eAircraft: Disrupting the way you fly!"[Online]. Available: https://www.ie-net.be/sites/default/files/Siemens%20eAircraft%20-%20Disrupting%20Aircraft%20Propulsion%20%20OO%20JH%20THO%20-%2020180427.cleaned.pdf

[93] N. Oswald, B. H. Stark, D. Holliday, C. Hargis and B. Drury, "Analysis of Shaped Pulse Transitions in Power Electronic Switching Waveforms for Reduced EMI Generation," *IEEE Trans. Ind. Appl*., vol. 47, no. 5, pp. 2154-2165, Sept.-Oct. 2011.

[94] D. Han, S. Li, Y. Wu, W. Choi and B. Sarlioglu, "Comparative Analysis on Conducted CM EMI Emission of Motor Drives: WBG Versus Si Devices," *IEEE Trans. Ind. Electron.*, vol. 64, no. 10, pp. 8353-8363, Oct. 2017.

[95] X. Gong and J. A. Ferreira, "Comparison and Reduction of Conducted EMI in SiC JFET and Si IGBT-Based Motor Drives," *IEEE Trans. Power Electron.*, vol. 29, no. 4, pp. 1757-1767, Apr. 2014.

[96] X. Gong, I. Josifović and J. A. Ferreira, "Modeling and Reduction of Conducted EMI of Inverters With SiC JFETs on Insulated Metal Substrate," *IEEE Trans. Power Electron*., vol. 28, no. 7, pp. 3138-3146, Jul. 2013.

[97] X. Gong and J. A. Ferreira, "Investigation of Conducted EMI in SiC JFET Inverters Using Separated Heat Sinks," *IEEE Trans. Ind. Electron*., vol. 61, no. 1, pp. 115-125, Jan. 2014.

[98] N. Oswald, P. Anthony, N. McNeill and B. H. Stark, "An Experimental Investigation of the Tradeoff between Switching Losses and EMI Generation With Hard-Switched All-Si, Si-SiC, and All-SiC Device Combinations," *IEEE Trans. Power Electron*., vol. 29, no. 5, pp. 2393-2407, May 2014.

[99] D. Han, C. T. Morris, W. Lee and B. Sarlioglu, "Comparison Between Output CM Chokes for SiC Drive Operating at 20- and 200-kHz Switching Frequencies," *IEEE Trans. Ind. Appl*., vol. 53, no. 3, pp. 2178-2188, May-Jun. 2017.

[100] D. Han, W. Lee, S. Li and B. Sarlioglu, "New Method for Common Mode Voltage Cancellation in Motor Drives: Concept, Realization, and Asymmetry Influence," *IEEE Trans. Power Electron*., vol. 33, no. 2, pp. 1188-1201, Feb. 2018.

[101] L. Wang, Y. Shi and H. Li, "Anti-EMI Noise Digital Filter Design for a 60-kW Five-Level SiC Inverter Without Fiber Isolation," *IEEE Trans. Power Electron*., vol. 33, no. 1, pp. 13-17, Jan. 2018.

[102] Z. Fang, D. Jiang and Y. Zhang, "Study of the characteristics and suppression of EMI of inverter with SiC and Si devices," *Chinese J. Electr. Engineering*, vol. 4, no. 3, pp. 37-46, Sep. 2018.

[103] D. Han, S. Li, W. Choi and B. Sarlioglu, "Design, implementation, and evaluation of a GaN-based four-leg inverter with minimal common mode voltage generation," in *Proc. IEEE Energy Conversion Congress and Exposition (ECCE)*, Cincinnati, OH, 2017, pp. 5383-5388.

[104] X. Gong, I. Josifovic and J. A. Ferreira, "Comprehensive CM filter design to suppress conducted EMI for SiC-JFET motor drives," in *Proc. 8th Int. Conf. Power Electron. - ECCE Asia*, Jeju, 2011, pp. 720-727.

[105] C. Morris, D. Han, W. Choi and B. Sarlioglu, "Evaluation of a novel common mode EMI reducing inverter topology utilizing wide bandgap

devices," in *Proc. IEEE Transportation Electrific. Conf. Expo. (ITEC)*, Chicago, IL, 2017, pp. 567-572.

[106] S. Narasimhan, S. Tewari, E. Severson, R. Baranwal and N. Mohan, "Mitigation of common-mode noise in wide band gap device based motor drives," in *Proc. IEEE Appl. Power Electron. Conf. Expo. (APEC)*, Long Beach, CA, 2016, pp. 2043-2050.

[107] D. Han, W. Lee, S. Li and B. Sarlioglu, "Comparative performance evaluation of common mode voltage reduction three-phase inverter topologies," in *Proc. IEEE Appl. Power Electron. Conf. Expo. (APEC)*, San Antonio, TX, 2018, pp. 2625-2629.

[108] Y. Jiang, W. Wu, Y. He, H. S. H. Chung and F. Blaabjerg, "New Passive Filter Design Method for Overvoltage Suppression and Bearing Currents Mitigation in a Long Cable Based PWM Inverter-Fed Motor Drive System," *IEEE Trans. Power Electron*., vol. 32, no. 10, pp. 7882-7893, Oct. 2017.

[109] Yifan Tang, "Analysis of steep-fronted voltage distribution and turn insulation failure in inverter-fed form-wound AC motor," *IEEE Trans. Ind. Appl*., vol. 34, no. 5, pp. 1088-1096, Sep/Oct 1998.

[110] B. Bai, Y. Wang and X. Wang, "Suppression for Discharging Bearing Current in Variable-Frequency Motors Based on Electromagnetic Shielding Slot Wedge," *IEEE Trans. Magn*., vol. 51, no. 11, pp. 1-4, Nov. 2015.

[111] M. M. Swamy, J. K. Kang and K. Shirabe, "Power Loss, System Efficiency, and Leakage Current Comparison Between Si IGBT VFD and SiC FET VFD With Various Filtering Options," *IEEE Trans. Ind. Appl*., vol. 51, no. 5, pp. 3858-3866, Sept.-Oct. 2015.

[112] M. M. Swamy and M. A. Baumgardner, "New Normal Mode dv/dt Filter With a Built-In Resistor Failure Detection Circuit," *IEEE Trans. Ind. Appl*., vol. 53, no. 3, pp. 2149-2158, May-Jun. 2017.

[113] E. Velander *et al*., "An Ultralow Loss Inductorless dv/dt Filter Concept for Medium-Power Voltage Source Motor Drive Converters With SiC Devices," *IEEE Trans. Power Electron.*, vol. 33, no. 7, pp. 6072-6081, Jul. 2018.

[114] D. Aggeler, F. Canales, J. Biela and J. W. Kolar, "Dv/Dt-Control Methods for the SiC JFET/Si MOSFET Cascode," *IEEE Trans. Power Electron*., vol. 28, no. 8, pp. 4074-4082, Aug. 2013.

[115] F. Qi, M. Wang and L. Xu, "Investigation and Review of Challenges in a High-Temperature 30-kVA Three-Phase Inverter Using SiC MOSFETs," *IEEE Trans. Ind. Appl.*, vol. 54, no. 3, pp. 2483-2491, May-Jun. 2018.

[116] Hassan, Y. Savaria and M. Sawan, "Electronics and Packaging Intended for Emerging Harsh Environment Applications: A Review," *IEEE Trans. Very Large Scale Integr. (VLSI) Syst*., vol. PP, issue 99, May, 2018.

[117] S. Tanimoto and K. Matsui, "High Junction Temperature and Low Parasitic Inductance Power Module Technology for Compact Power Conversion Systems," *IEEE Trans. Electron Devices*, vol. 62, no. 2, pp. 258-269, Feb. 2015.

[118] Z. Shen, R. W. Johnson and M. C. Hamilton, "SiC Power Device Die Attach for Extreme Environments," *IEEE Trans. Electron Devices*, vol. 62, no. 2, pp. 346-353, Feb. 2015.

[119] R. Khazaka, L. Mendizabal, D. Henry and R. Hanna, "Survey of High-Temperature Reliability of Power Electronics Packaging Components," *IEEE Trans. Power Electron.*, vol. 30, no. 5, pp. 2456-2464, May 2015.

[120] R. Wang, Z. Chen, D. Boroyevich, L. Jiang, Y. Yao and K. Rajashekara, "A Novel Hybrid Packaging Structure for High-Temperature SiC Power Modules," *IEEE Trans. Ind. Appl.*, vol. 49, no. 4, pp. 1609-1618, Jul.-Aug. 2013.

[121] V. R. Manikam and K. Y. Cheong, "Die Attach Materials for High Temperature Applications: A Review," *IEEE Trans. Compon. Packag. Manuf. Technol.*, vol. 1, no. 4, pp. 457-478, Apr. 2011.

[122] L. Abbatelli, C. Brusca, and G. Catalisano, "How to fine tune your SiC MOSFET gate driver to minimize losses" [online] Available: http://www.st.com/content/ccc/resource/technical/document/application_note/7d/2b/9d/f0/88/07/4b/6f/DM00170577.pdf/files/DM00170577.pdf/jcr:content/translations/en.DM00170577.pdf on Jan. 8, 2018.

[123] A. Rujas, V. M. López, L. Mir and T. Nieva, "Gate driver for high power SiC modules: design considerations, development and experimental validation," *IET Power Electron.*, vol. 11, no. 6, pp. 977-983, 29 5 2018.

[124] P. Anthony, N. McNeill and D. Holliday, "High-Speed Resonant Gate Driver With Controlled Peak Gate Voltage for Silicon Carbide MOSFETs," *IEEE Trans. Ind. Appl.*, vol. 50, no. 1, pp. 573-583, Jan.-Feb. 2014.

[125] Z. Zeng and X. Li, "Comparative Study on Multiple Degrees of Freedom of Gate Drivers for Transient Behavior Regulation of SiC MOSFET," *IEEE Trans. Power Electron.*, vol. 33, no. 10, pp. 8754-8763, Oct. 2018.

[126] Z. Zhang, W. Zhang, F. Wang, L. M. Tolbert and B. J. Blalock, "Analysis of the switching speed limitation of wide band-gap devices in a phase-leg configuration," in *Proc. IEEE Energy Convers. Congr. Expo. (ECCE)*, Raleigh, NC, 2012, pp. 3950-3955.

[127] B. Zhang, S. Xie, J. Xu, Q. Qian, Z. Zhang and K. Xu, "A Magnetic Coupling Based Gate Driver for Crosstalk Suppression of SiC MOSFETs," *IEEE Trans. Ind. Electron.*, vol. 64, no. 11, pp. 9052-9063, Nov. 2017.

[128] F. Gao, Q. Zhou, P. Wang and C. Zhang, "A Gate Driver of SiC MOSFET for Suppressing the Negative Voltage Spikes in a Bridge Circuit," *IEEE Trans. Power Electron.*, vol. 33, no. 3, pp. 2339-2353, Mar. 2018.

[129] Z. Zhang, J. Dix, F. F. Wang, B. J. Blalock, D. Costinett and L. M. Tolbert, "Intelligent Gate Drive for Fast Switching and Crosstalk Suppression of SiC Devices," *IEEE Trans. Power Electron.*, vol. 32, no. 12, pp. 9319-9332, Dec. 2017.

[130] P. Nayak and K. Hatua, "Active Gate Driving Technique for a 1200 V SiC MOSFET to Minimize Detrimental Effects of Parasitic Inductance in the Converter Layout," *IEEE Trans. Ind. Appl.*, vol. 54, no. 2, pp. 1622-1633, Mar.-Apr. 2018.

[131] P. Nayak and K. Hatua, "Parasitic Inductance and Capacitance-Assisted Active Gate Driving Technique to Minimize Switching Loss of SiC MOSFET," *IEEE Trans. Ind. Electron.*, vol. 64, no. 10, pp. 8288-8298, Oct. 2017.

[132] H. C. P. Dymond *et al*., "A 6.7-GHz Active Gate Driver for GaN FETs to Combat Overshoot, Ringing, and EMI," *IEEE Trans. Power Electron.*, vol. 33, no. 1, pp. 581-594, Jan. 2018.

[133] J. V. P. S. Chennu, R. Maheshwari and H. Li, "New Resonant Gate Driver Circuit for High-Frequency Application of Silicon Carbide MOSFETs," *IEEE Trans. Ind. Electron.*, vol. 64, no. 10, pp. 8277-8287, Oct. 2017.

[134] P. Nayak, S. K. Pramanick and K. Rajashekara, "A High-Temperature Gate Driver for Silicon Carbidemosfet," *IEEE Trans. Ind. Electron.*, vol. 65, no. 3, pp. 1955-1964, Mar. 2018.

[135] Z. Wang *et al*., "A High Temperature Silicon Carbide mosfet Power Module With Integrated Silicon-On-Insulator-Based Gate Drive," *IEEE Trans. Power Electron.*, vol. 30, no. 3, pp. 1432-1445, Mar. 2015.

[136] F. Qi and L. Xu, "Development of a High-Temperature Gate Drive and Protection Circuit Using Discrete Components," *IEEE Trans. Power Electron.*, vol. 32, no. 4, pp. 2957-2963, Apr. 2017.

[137] G. Engelmann, T. Senoner and R. W. De Doncker, "Experimental investigation on the transient switching behavior of SiC MOSFETs using a stage-wise gate driver," *CPSS Trans. Power Electron. Appl.*, vol. 3, no. 1, pp. 77-87, Mar. 2018.

[138] Z. Zhang, F. Wang, L. M. Tolbert and B. J. Blalock, "Active Gate Driver for Crosstalk Suppression of SiC Devices in a Phase-Leg Configuration," *IEEE Trans. Power Electron*., vol. 29, no. 4, pp. 1986-1997, Apr. 2014.

[139] Y. Li, M. Liang, J. Chen, T. Q. Zheng and H. Guo, "A Low Gate Turn-off Impedance Driver for Suppressing Crosstalk of SiC MOSFET Based on Different Discrete Package," *IEEE J. Emerg. Sel. Topics Power Electron*.

[140] Y. Han, H. Lu, Y. Li and J. Chai, "Open-Loop Gate Control for Optimizing the Turn-On Transition of SiC MOSFETs," *IEEE J. Emerg. Sel. Topics Power Electron*.

[141] A. Anurag, S. Acharya, Y. Prabowo, G. Gohil and S. Bhattacharya, "Design Considerations and Development of an Innovative Gate Driver for Medium Voltage Power Devices with High dv/dt," *IEEE Trans. Power Electron*.

[142] Wolfspeed SiC Power Modules [Online]. Available: https://www.wolfspeed.com/power/products/sic-power-modules

[143] X. She *et al*., "High Performance Silicon Carbide Power Block for Industry Applications," *IEEE Trans. Ind. Appl*., vol. 53, no. 4, pp. 3738-3747, Jul.-Aug. 2017.

[144] J. Colmenares, D. Peftitsis, J. Rabkowski, D. Sadik, G. Tolstoy and H. Nee, "High-Efficiency 312-kVA Three-Phase Inverter Using Parallel Connection of Silicon Carbide MOSFET Power Modules," *IEEE Trans. Ind. Appl.*, vol. 51, no. 6, pp. 4664-4676, Nov.-Dec. 2015.

[145] F. Qi, M. Wang and L. Xu, "Investigation and Review of Challenges in a High-Temperature 30-kVA Three-Phase Inverter Using SiC MOSFETs," *IEEE Trans. Ind. Appl*., vol. 54, no. 3, pp. 2483-2491, May-Jun. 2018.

[146] E. Gurpinar, F. Iannuzzo, Y. Yang, A. Castellazzi and F. Blaabjerg, "Design of Low-Inductance Switching Power Cell for GaN HEMT Based Inverter," *IEEE Trans. Ind. Appl*., vol. 54, no. 2, pp. 1592-1601, Mar.-Apr. 2018.

[147] X. Zhang, N. Haryani, Z. Shen, R. Burgos and D. Boroyevich, "Ultra-low inductance phase leg design for GaN-based three-phase motor drive systems," in *Proc. IEEE 3rd Workshop on Wide Bandgap Power Devices and Appl. (WiPDA)*, Blacksburg, VA, 2015, pp. 119-124.

[148] J. Lautner and B. Piepenbreier, "Evaluation of GaN transistors in a phase-leg configuration for motor drive applications," in *Proc. 19th Eur. Conf. Power Electron. Appl. (EPE'17 ECCE Europe)*, Warsaw, 2017, pp. P.1-P.9.

[149] D. Othman, M. Berkani, S. Lefebvre, A. Ibrahim, Z. Khatir, and A. Bouzourene, "Comparison study on performances and robustness between SiC MOSFET & JFET devices–Abilities for aeronautics application," *Eur. Symp. Reliab. Electron Devices, Failure Phys. Anal.*, vol. 52, no. 9, pp. 1859–1964, Sep. 2012.

[150] Z. Wang *et al*., "Temperature-Dependent Short-Circuit Capability of Silicon Carbide Power MOSFETs," *IEEE Trans. Power Electron.*, vol. 31, no. 2, pp. 1555-1566, Feb. 2016.

[151] G. Romano *et al*., "A Comprehensive Study of Short-Circuit Ruggedness of Silicon Carbide Power MOSFETs," *IEEE J. Emerg. Sel. Topics Power Electron.*, vol. 4, no. 3, pp. 978-987, Sep. 2016.

[152] Z. Wang, X. Shi, Y. Xue, L. M. Tolbert, F. Wang and B. J. Blalock, "Design and Performance Evaluation of Overcurrent Protection Schemes for Silicon Carbide (SiC) Power MOSFETs," *IEEE Trans. Ind. Electron*., vol. 61, no. 10, pp. 5570-5581, Oct. 2014.

[153] D. Sadik *et al*., "Short-Circuit Protection Circuits for Silicon-Carbide Power Transistors," *IEEE Trans. Ind. Electron.*, vol. 63, no. 4, pp. 1995-2004, Apr. 2016.

[154] L. Fursin, X. Li, Z. Li, M. O'Grady, W. Simon and A. Bhalla, "Reliability aspects of 1200V and 3300V silicon carbide MOSFETs," in *Proc. IEEE 5th Workshop on Wide Bandgap Power Devices and Appl. (WiPDA)*, Albuquerque, NM, 2017, pp. 373-377.

[155] T. H. Duong, J. M. Ortiz, D. W. Berning, A. R. Hefner, S. -. Ryu and J. W. Palmour, "Electro-thermal simulation of 1200 V 4H-SiC MOSFET short-circuit SOA†," in *Proc. IEEE 27th Int. Symp. Power Semicond. Devices & IC's (ISPSD)*, Hong Kong, 2015, pp. 217-220.

[156] A. Castellazzi, A. Fayyaz, L. Yang, M. Riccio and A. Irace, "Short-circuit robustness of SiC Power MOSFETs: Experimental analysis," in *Proc. IEEE 26th Int. Symp. Power Semicond. Devices & IC's (ISPSD)*, Waikoloa, HI, 2014, pp. 71-74.

[157] A. Kadavelugu, E. Aeloiza and C. Belcastro, "Short-circuit performance of multi-chip SiC MOSFET modules," in *Proc. IEEE 5th Workshop on Wide Bandgap Power Devices and Appl. (WiPDA)*, Albuquerque, NM, 2017, pp. 285-290.

[158] S. Ji *et al*., "Short circuit characterization of 3rdgeneration 10 kV SiC MOSFET," in *Proc. IEEE Appl. Power Electron. Conf. Expo. (APEC)*, San Antonio, TX, 2018, pp. 2775-2779.

[159] K. Tani, J. Sakano and A. Shima, "Analysis of short-circuit break-down point in 3.3 kV SiC-MOSFETs," in *Proc. IEEE 30th Int. Symp. Power Semicond. Devices and ICs (ISPSD)*, Chicago, IL, 2018, pp. 383-386.

[160] T. Horiguchi, S. Kinouchi, Y. Nakayama and H. Akagi, "A fast short-circuit protection method using gate charge characteristics of SiC MOSFETs," in *Proc. IEEE Energy Convers. Congr. Expo. (ECCE)*, Montreal, QC, 2015, pp. 4759-4764.

[161] H. Li *et al*., "E-mode GaN HEMT short circuit robustness and degradation," in *Proc. 2017 IEEE Energy Convers. Congr. Expo. (ECCE)*, Cincinnati, OH, 2017, pp. 1995-2002.

[162] M. Fernández *et al*., "Short-Circuit Study in Medium-Voltage GaN Cascodes, p-GaN HEMTs, and GaN MISHEMTs," *IEEE Trans. Ind. Electron.*, vol. 64, no. 11, pp. 9012-9022, Nov. 2017.

[163] M. Fernández *et al*., "P-GaN HEMTs Drain and Gate Current Analysis Under Short-Circuit," *IEEE Electron Device Lett.*, vol. 38, no. 4, pp. 505-508, Apr. 2017.

[164] R. Hou, J. Lu, and D. Chen,"An Ultrafast Discrete Short-Circuit Protection Circuit for GaN HEMTs" in *Proc. IEEE Energy Convers. Congr. Expo. (ECCE)*, Portland, OR, 2018.

[165] D. J. Lichtenwalner *et al*., "Reliability studies of SiC vertical power MOSFETs," in *proc*. *IEEE Int. Reliab. Physics Symp. (IRPS)*, Burlingame, CA, 2018, pp. 2B.2-1-2B.2-6.

[166] R. E. Stahbush and N. A. Mahadik, "Defects affecting SiC power device reliability," in *proc*. *IEEE Int. Reliab. Physics Symp. (IRPS)*, Burlingame, CA, 2018, pp. 2B.4-1-2B.4-4.

[167] X. Zhou, H. Su, Y. Wang, R. Yue, G. Dai and J. Li, "Investigations on the Degradation of 1.2-kV 4H-SiC MOSFETs Under Repetitive Short-Circuit Tests," *IEEE Trans. Electron Devices*, vol. 63, no. 11, pp. 4346-4351, Nov. 2016.

[168] A. J. Lelis, R. Green and D. B. Habersat, "SiC MOSFET reliability and implications for qualification testing," in *proc*. *IEEE Int. Reliab. Physics Symp. (IRPS)*, Monterey, CA, 2017, pp. 2A-4.1-2A-4.4.

[169] D. A. Gajewski *et al*., "SiC power device reliability," in *proc*. *IEEE Int. Integr. Reliab. Workshop (IIRW)*, South Lake Tahoe, CA, 2016, pp. 29-34.

[170] J. B. Casady *et al*., "First automotive reliability assessment and drive-train performance of large-area 900V, 10mOhm SiC MOSFETs," in *proc*. *IEEE Applied Power Electron. Conf. Expo. (APEC)*, Tampa, FL, 2017, pp. 2259-2262.

[171] "New Wolfspeed Silicon Carbide Semiconductors First to Meet Automotive AEC-Q101 Standards" [Online]. Available: https://www.wolfspeed.com/news/new-wolfspeed-silicon-carbide-semiconductors-first-to-meet-automotive-aec-q101-standards

[172] P. Losee *et al*., "1.2kV class SiC MOSFETs with improved performance over wide operating temperature," in *Proc. 26th Int. Symp. on Power Semicond. Devices & IC's (ISPSD)*, Waikoloa, HI, Jun. 2014, pp. 297-300.

[173] M. Meneghini *et al*., "Reliability and failure analysis in power GaN-HEMTs: An overview," in *proc*. *IEEE Int. Reliab. Physics Symp. (IRPS)*, Monterey, CA, 2017, pp. 3B-2.1-3B-2.8.

[174] C. Liu *et al*., "Breakthroughs for 650-V GaN Power Devices: Stable high-temperature operations and avalanche capability," *IEEE Power Electron. Mag.* , vol. 2, no. 3, pp. 44-50, Sep. 2015.

[175] A. Lidow, R. Strittmatter, C. Zhou and Y. Ma, "Enhancement mode gallium nitride transistor reliability," in *proc*. *IEEE Int. Reliab. Physics Symp*., Monterey, CA, 2015, pp. 2E.1.1-2E.1.5.

[176] A. Lidow, J. Strydom, R. Strittmatter and C. Zhou, "GaN: A Reliable Future in Power Conversion: Dramatic performance improvements at a lower cost," *IEEE Power Electron. Mag*., vol. 2, no. 1, pp. 20-26, Mar. 2015.

[177] G. Patterson and J. Roberts, "Gallium nitride - delivering its promise in automotive applications," in *proc*. *6th Hybrid and Elect. Vehicles Conf. (HEVC)*, London, 2016, pp. 1-6.